

# Three-Dimensional Graphene-Based Structures: Production Methods, Properties, and Applications

Leila Haghghi Poudeh<sup>1,2</sup>, Mehmet Yildiz<sup>1,2</sup>, Yusuf Menciloglu<sup>1,2</sup> and Burcu Saner Okan<sup>2\*</sup>

<sup>1</sup>Faculty of Engineering and Natural Sciences, Materials Science and Nano Engineering, Sabanci University, Orhanli-Tuzla, Istanbul, Turkey

<sup>2</sup>Sabanci University Integrated Manufacturing Technologies Research and Application Center & Composite Technologies Center of Excellence, Teknopark İstanbul, Pendik, İstanbul, Turkey

---

## Abstract

Graphene, a two-dimensional (2D)  $sp^2$ -hybridized carbon sheet, shows excellent chemical, mechanical, and physical properties owing to its unique structure, which makes it a great potential in the energy storage devices, sensors, composite materials, and biotechnology. The utilization of graphene sheets into the macroscopic structures is one of the important issues since 2D graphene sheets tend to restack together in bulk materials due to strong  $\pi$ - $\pi$  interactions and van der Waals forces. The aggregation of graphene sheets and their crumbling lead to a significant decrease in electrical conductivity, surface area, and mechanical strength which negatively affects the utilization of graphene in the practical applications. Recently, three-dimensional (3D) graphene materials have been attracting much attention since they not only preserve the intrinsic properties of 2D graphene sheets by inhibiting the agglomeration behavior of 2D graphene sheets but also provide advanced functions with improved performance in various applications.

The content of this chapter covers (i) a brief summary of production techniques of 2D graphene and its drawbacks, (ii) main strategies for the development of 3D graphene structures, (iii) production methods, and (iv) possible applications of 3D graphene architectures in composites and energy-storage devices.

**Keywords:** Three-dimensional graphene, crumbling, energy storage devices, composites

## 11.1 Introduction

Graphene, a two-dimensional (2D) hexagonal lattice of  $sp^2$  carbon atoms, has been the interest of many studies. The long-range  $\pi$ -conjugation in graphene yields intriguing properties such as high electrical and thermal conductivity [1, 2], large surface area [3], good chemical stability [4], and excellent mechanical strength [5], which make it a great candidate in various applications such as energy storage systems, polymer composites, and sensors [3]. However, in practical applications, 2D graphene sheets tend to restack

---

\*Corresponding author: bsanerokan@sabanciuniv.edu

together due to strong  $\pi$ - $\pi$  interactions and van der Waals forces, which lead to a significant decrease in electrical conductivity and surface area, and this affects negatively the utilization of graphene in many fields. To overcome this problem and provide advanced functions with improved performance, several 3D graphene structures such as graphene networks [6], graphene fibers [7], and graphene spheres [8] have been constructed. The combination of 3D structures and intrinsic properties of graphene provide high surface area, excellent mechanical strength, and fast mass and electron transport for the 3D graphene architectures. So far, many studies have focused on the fabrication of different 3D graphene structures by using different methods. In general, there are two main routes for the synthesis of 3D graphene structures: i) assembly of 2D graphene sheets and ii) direct synthesis of 3D graphene [9]. The proper choice of the fabrication method relies on the desired quality and quantity of graphene. While some applications need high-quality graphene such as in the electronic devices and sensors, other fields like polymer composites and energy storage devices are in the demand of comparably large quantities of graphene.

This chapter initially focuses on the main routes and recent progresses in the synthesis of 3D graphene architectures. At the second part of the chapter, different morphologies of 3D graphene and their potential applications are discussed in detail.

## 11.2 Preparation of Graphene

Graphene was first fabricated *via* micromechanical exfoliation of graphite [10]. By using this approach, it is possible to obtain single- or few-layer graphene sheets with high quality. However, this technique is not suitable for mass production. To address this problem, several alternative techniques including bottom-up and top-down approaches have been developed in order to synthesize 2D graphene sheets. Epitaxial growth [11] and chemical vapor deposition (CVD) method [12] are the most widely used bottom-up techniques, whereas top-down approach includes electrochemical exfoliation [13] and chemical exfoliation of graphite oxide [14]. Among top-down methods, chemical approach has attracted great interest because of easy processability and large-scale production; thus it could be utilized in many applications [15]. On the other hand, chemically derived 2D graphene sheets are the main component for the construction of 3D graphene structures [16]. This technique involves the oxidation of graphite, followed by the exfoliation process in order to obtain graphene oxide (GO) [17]. Figure 11.1 shows the schematic representation of the different methods for the fabrication of graphene [18]. Many studies have focused on the oxidation of graphite into graphite oxide. Brodie [19] first reported the synthesis of graphite oxide in the presence of potassium chlorate and nitric acid. Later, Staudenmaier [20] improved the procedure by adding concentrated sulfuric acid ( $\text{H}_2\text{SO}_4$ ) to the mixture. However, this method was time consuming and hazardous. In 1958, Hummers [21] used a combination of potassium permanganate and concentrated  $\text{H}_2\text{SO}_4$  in the presence of sodium nitrate. So far, Hummers method with some modifications and improvements is the most common used route for the synthesis of graphite oxide [22, 23]. The synthesized graphite oxide is then exfoliated into single- or few-layered GO sheets dispersed in aqueous solutions or expanded by applying heat treatment [24]. Finally, graphene oxide is reduced to graphene sheets by applying thermal annealing [25] or using reducing agents such as hydrazine [26], hydroquinone [27], and sodium borohydride [28].

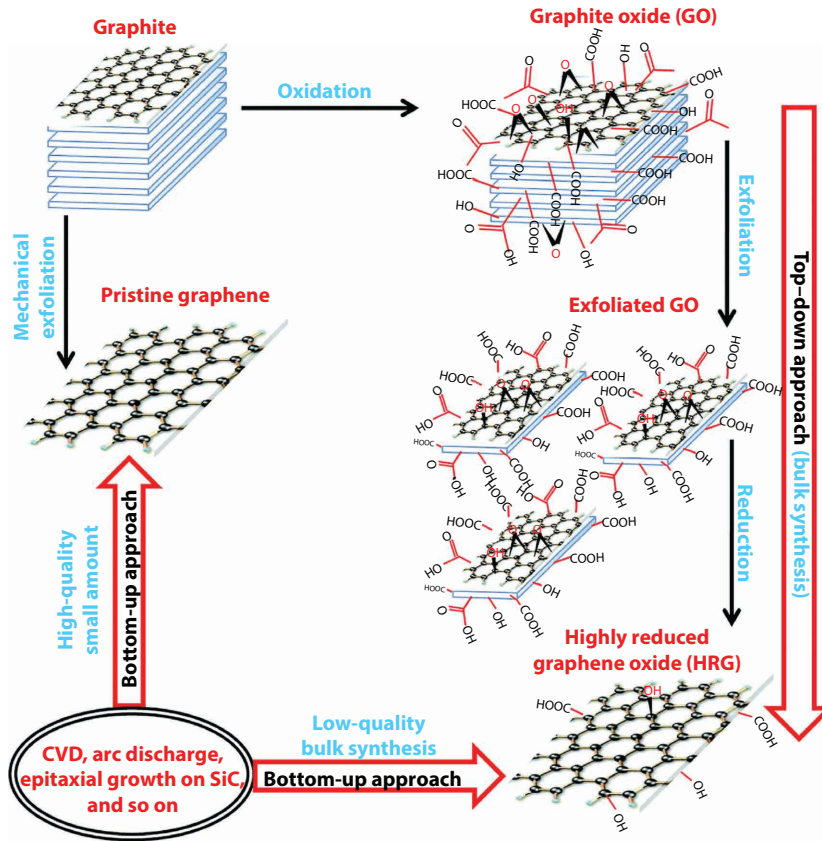


**Figure 11.1** Schematic representation of the methods used for the synthesis of graphene, which are classified into top-down and bottom-up approaches. The top-down approach is widely used for the scalable synthesis of graphene that produces a relatively low quality of a graphene-like material commonly known as reduced graphene oxide (rGO) or graphene in large quantity required for the preparation of graphene-based nanocomposites [18]. (Reproduced with permission of Royal Society of Chemistry.)

### 11.3 Preparation Methods of 3D Graphene Architectures

In the past few years, large efforts have been devoted to the utilization of 3D graphene materials with different morphologies and functionalities. In this section, the preparation methods of 3D graphene structures are classified as assembly of GO sheets by using different techniques and direct deposition of 3D graphene architectures through CVD. All the methods and recent studies have been discussed in detail.

#### 11.3.1 Assembly of GO Sheets

Assembly method is one of promising strategies for the construction of 3D graphene architectures because of its distinct advantages including high yield, low cost, and easy functionalization of graphene [29]. In this technique, GO solution is preferred over graphene since GO behaves like an amphiphilic material with hydrophilic edges and hydrophobic basal plane [30]. Therefore, it could easily make a stable dispersion in aqueous solutions.

At the final step of assembly technique and in order to obtain 3D graphene architectures, GO sheets are reduced whether by chemical routes or thermal annealing to the reduced graphene (rGO) [31]. It should be noted that the driving force behind formation of the 3D graphene architectures *via* assembly method are the interactions like van der Waals forces, hydrogen bonding, dipole interactions, electrostatic interactions, and  $\pi$ - $\pi$  stacking [32].

### 11.3.1.1 Self-Assembly Method

Self-assembly is one of the most widely used techniques that converts 2D graphene sheets to 3D macroscopic graphene architectures with different functionalities. The obtained structures have great potentials to be used in various applications such as energy storage devices [33], medicine [34], and optoelectronics [35]. In this technique, 3D graphene structures are obtained through the gelation of GO dispersion followed by the reduction process of GO to rGO [31]. Basically, in colloidal chemistry, gelation occurs when the electrostatic forces between colloids are changed [36]. In the case of stable GO dispersion, there is a force balance between the van der Waals attractions of GO basal planes and the repulsion forces of functional groups of GO sheets. Once this force balance is broken, gelation process is started and subsequently GO sheets overlap and form different GO morphologies such as hydrogels, organogels, or aerogels, which are physically or chemically linked to each other [37, 38]. At the final step, GO hydrogels are reduced to form 3D graphene networks. There are many ways to initiate the gelation process of a stable GO dispersion. For example, additive-free GO hydrogels were fabricated by changing the pH of dispersion [31] and applying ultrasonication technique [39]. During sonication, GO sheets are fractured to the smaller sheets. As a result, produced new edges contain nonstabilized carboxyl groups. This change in the surface of GO initiates the gelation (Figure 11.2a, b). Moreover, the

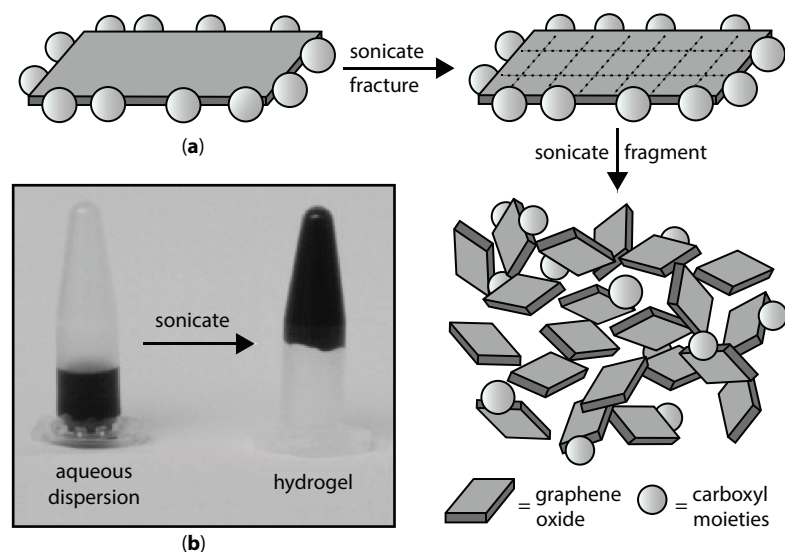


**Figure 11.2** (a) Diagram illustrating the fracture and fragmentation of GO sheets during sonication, where reduced coverage of carboxyl moieties (represented as spheres) along the edges of the sheets fragments leads to gelation. (b) Digital image demonstrating the conversion of an as-prepared aqueous graphene oxide dispersion (left) into a hydrogel (right) after sonication [39]. (Reproduced with permission of Elsevier.)

addition of cross-linkers like polyvinyl alcohol (PVA) [40], DNA [41], and metal ions [42] to the solution can trigger the gelation process. Bai and co-workers [40] reported the synthesis of GO hydrogel by the addition of PVA, a water-soluble polymer, as a cross-linker to the aqueous GO solution. The hydrogen bonding interactions between hydroxyl-rich polymeric chains and oxygen functional groups of GO form cross-linking sites and thus fabricate GO hydrogels.

On the other hand, 3D graphene architectures can be directly obtained by the self-assembly of GO sheets *via* hydrothermal or chemical reduction processes. In these techniques, GO sheets are directly self-assembled and reduced to rGO at the same time [37]. For instance, an electrically conductive and porous 3D graphene network has been prepared *via* mild chemical reduction of GO by sodium bisulfide at 95°C under atmospheric pressure and in the presence of iron oxide nanoparticles [43]. He *et al.* [44] reported the facile fabrication of 3D graphene sponges containing palladium and indium by combination of the hydrothermal and chemical reduction techniques. In this study, GO aqueous solution containing palladium and indium salts and vitamin C as reducing agent were treated hydrothermally at 110°C for 6 h.

Generally, after gelation and reduction of 3D graphene architectures, a drying procedure is needed to remove the water and organic molecules from the structure while preserving the main framework [45]. Freeze-drying as one of the feasible drying techniques is usually applied as the final step of the assembly methods. By using this technique, it is possible to fabricate highly porous structures with improved mechanical and electrical properties since the pore size could be controlled by monitoring the process parameters like temperature [46]. Figure 11.3 shows the SEM images of 3D graphene structures which are freeze-dried at different temperatures [46].

Alternatively, electrochemical reduction as a well-known route is usually used to deposit active materials like 3D graphene architectures on the surface of the electrodes [47]. Chen *et al.* [48] fabricated 3D porous graphene-based composites involving two electrochemical deposition steps. As shown in Figure 11.4, GO sheets were first electrochemically reduced to a porous 3D graphene framework, and then three different components as conductive polymers, noble metals, and metal oxides were integrated to the 3D porous graphene

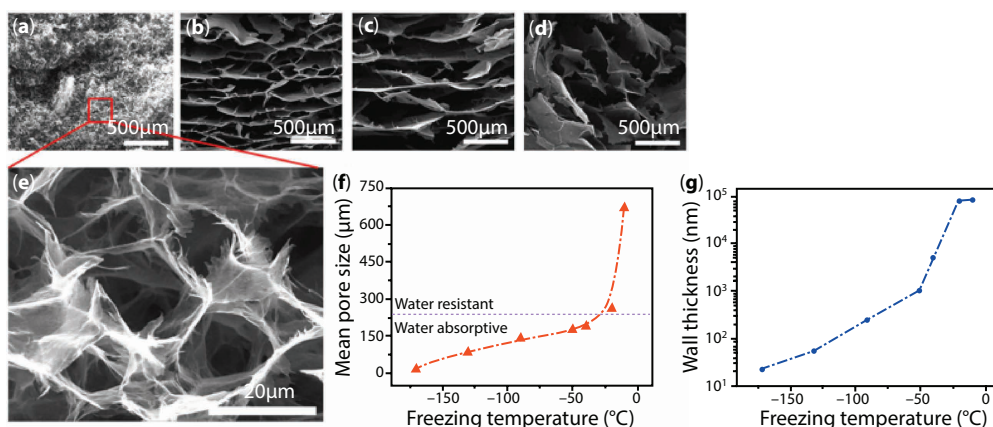


**Figure 11.3** (a–d) Microstructures of sponge graphenes frozen at different temperatures of  $-170^{\circ}\text{C}$ ,  $-40^{\circ}\text{C}$ ,  $-20^{\circ}\text{C}$ , and  $-10^{\circ}\text{C}$ , respectively. (e) High-magnification SEM image of the pore walls composed of graphene nanosheets corresponding to panel a. The mean thickness of the pore walls is 10 nm. (f) Statistics of the average pore size, and (g) Wall thickness as a function of freezing temperature. Mean pore size varies from 10 to 700 nm [46]. (Reproduced with permission of Springer Nature.)

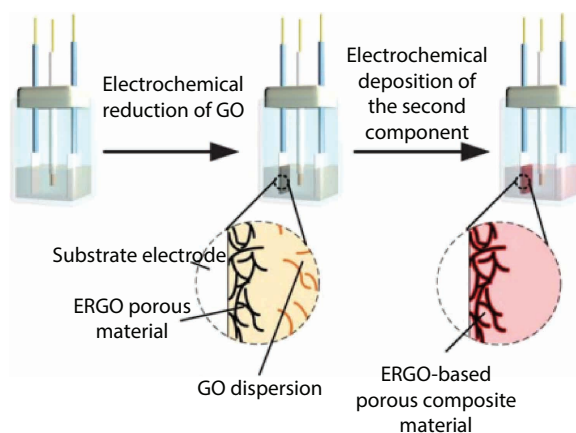


**Figure 11.4** Schematic illustration of the self-assembly of GO sheets using electrochemical deposition [48]. (Reproduced with permission of Royal Society of Chemistry.)

network, separately *via in situ* electrochemical deposition. Electrochemically deposited 3D graphene-based architectures can be directly used in the electrochemical devices as high-performance electrode materials.

### 11.3.1.2 Template-Assisted Method

3D graphene architectures can be fabricated with another feasible and convenient way by using pre-designed 3D templates such as polystyrene (PS) [49] and silicon dioxide ( $\text{SiO}_2$ ) [50] following by the reduction of GO and removing the template from the structure. Generally, the used template is surrounded by graphene sheets by electrostatic interactions between negatively charged graphene sheets and positively charged template. Compared to self-assembly strategy, with this technique, it is possible to obtain more controlled structure with desirable morphology [37]. However, the size of architectures directly depends on the size of templates [8]. So far, considerable amounts of work have focused on the production of 3D graphene-based materials using template-assisted method. In one of the works, as shown in Figure 11.5a, positively charged PS spheres as template were coated with GO sheets followed by the reduction of GO to rGO by using hydrazine. Finally, graphene hollow spheres were fabricated after calcination at  $420^\circ\text{C}$  for 2 h to remove PS from the core [51]. Wu *et al.* [52] reported a facile synthesis route for the fabrication of graphene-based hollow spheres as electrocatalysts for oxygen reduction. As shown in Figure 11.5b, strong electrostatic interactions between polyethylenimine functionalized  $\text{SiO}_2$  spheres and graphene sheets result in the formation of GO- $\text{SiO}_2$  spherical particles. After reduction process and washing with hydrofluoric acid, graphene-based hollow spheres were obtained.

In an effort to produce 3D graphene architectures with more controlled manner, Huang and coworkers [53] reported a facile assembly method of porous graphene foams with controlled pore sizes with the help of hydrophobic interactions of GO sheets and functionalized  $\text{SiO}_2$  spherical templates followed by the calcination and silica etching. Figure 11.6 represents the schematic illustration of synthesis procedure of the nanoporous graphene foam with a controllable pore size of 30–120 nm.

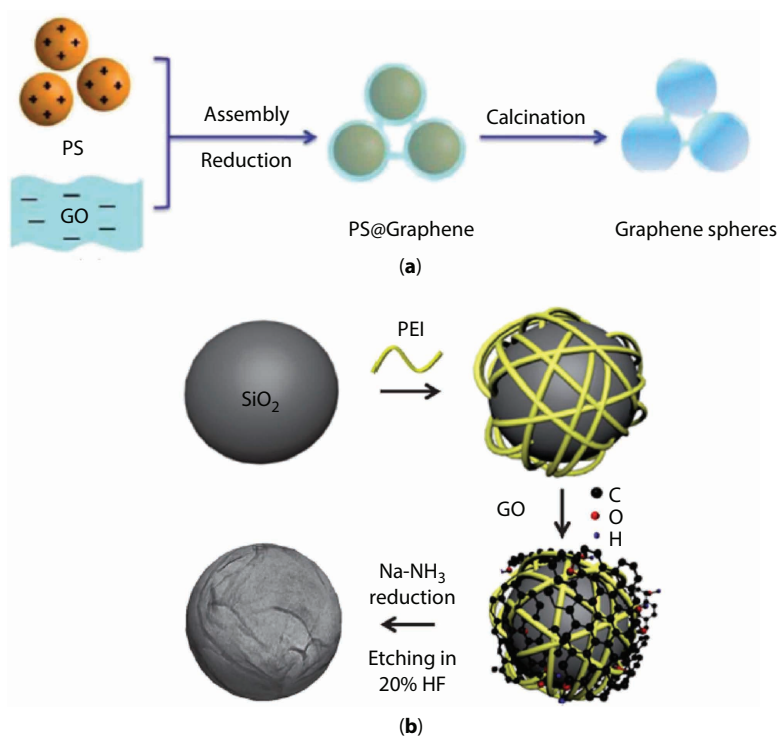


**Figure 11.5** Schematic illustrations of the fabrication procedure of graphene-based hollow spheres using (a) PS [51] and (b)  $\text{SiO}_2$  [52] as template. (Reproduced with permission of Royal Society of Chemistry.)

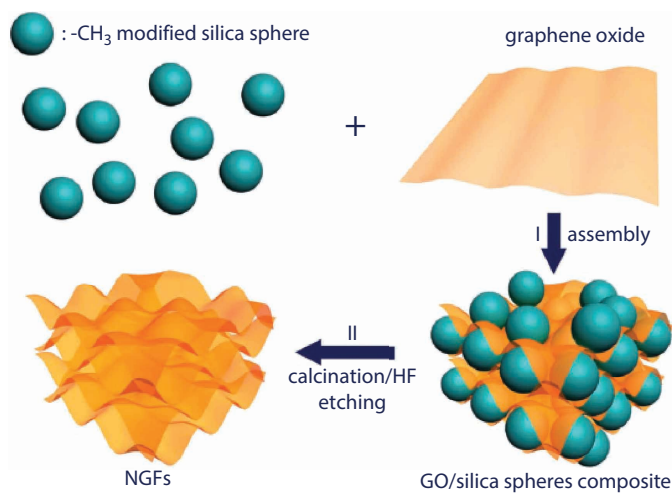


**Figure 11.6** Schematic illustration of the synthesis procedures of the nanoporous graphene foams. I) The self-assembly occurs between GOs and hydrophobic silica templates. II) Calcination and silica etching to produce NGFs [53]. (Reproduced with permission of Wiley.)

### 11.3.1.3 Electrospraying

Electrospinning/electrospraying is a simple and well-known technique to produce graphene-based fibers and spherical or bead-like structures with the diameters ranging from few micrometers to nanometer by adjusting the process parameters. In this process, a strong electric field is applied between a nozzle containing graphene-based solution and grounded metallic plate as a collector. When the surface tension of solution at the tip of the nozzle is overcome to the electric field, the droplet stretches and forms a continuous jet, which is collected as graphene-based fibers or spherical structures on the collector [54].

More recently, core-shell electrospinning/electrospraying has received great attention due to its possibility to attain multifunctionality and utilize different materials in one-step process by eliminating deposition steps as in the self-assembly and template-assisted methods, and thus it expands the potential applications of fabricated structures in many areas including drug delivery, energy storage, sensors, and nanocomposites [8, 55]. In this technique, the final morphology is affected by various solution properties (such as viscosity and electrical conductivity) and process parameters (such as voltage and flow rate) [56]. Up to now, there are lots of attempts for the integration of graphene into fiber structure using both classic and core-shell electrospinning technology [57–59]. However, very recently, Poudeh *et al.* [8] proposed a new design of 3D graphene-based hollow and filled polymeric spheres through one-step core-shell electrospaying technique. In this study, the proper polymer concentration for the sphere production was determined by using Mark–Houwink–Sakurada equations since proper polymer concentration and solution viscosity are required in order to obtain desired spherical morphology. In the case of hollowness, core material should contain a solvent with a high vapor pressure than the shell solution. Figure 11.7 represents the schematic illustration of fabrication of graphene-based spheres using core-shell electrospaying method, which eliminates crumbling, and agglomeration problem of 2D graphene sheets and provides better dispersion of graphene layers through polymeric chains. The possible interactions between the polymeric chains and graphene sheets during sphere formation are also shown in Figure 11.7 (left).

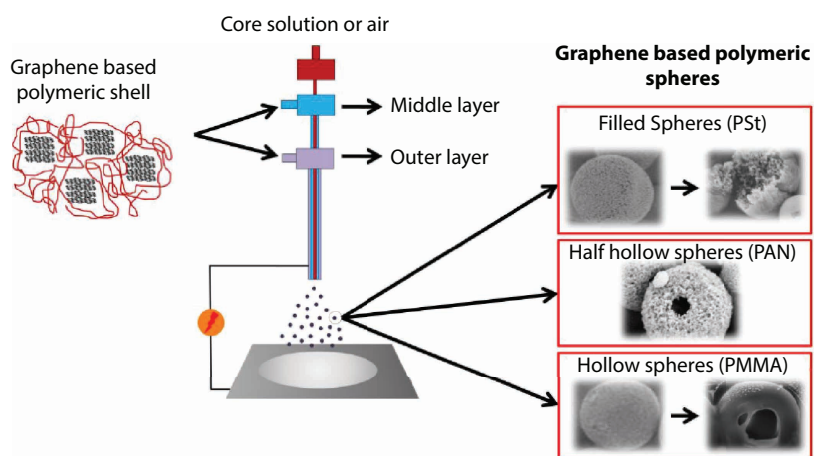


**Figure 11.7** Schematic illustration of fabrication of 3D graphene-based spheres using core-shell electrospaying technique and (left) possible interactions between polymeric chains and graphene sheets during sphere formation [8]. (Reproduced with permission of Royal Society of Chemistry.)

### 11.3.2 Direct Deposition of 3D Graphene Structures

Chemical vapor deposition (CVD) is a convenient method for the construction of 3D porous graphene networks with superior properties such as large surface area and high electrical conductivity comparable to that of pristine graphene [12]. Over and above this, in the aforementioned 3D graphene synthesis routes, chemically derived graphene is the starting material, and since during oxidation and reduction process of GO some defects are introduced to the system, the fabricated 3D graphene structures would exhibit low electrical conductivity when compared to 3D graphene structures growth with CVD. In this method, graphene directly grows from organic precursors on a substrate [60]. Compared to the classical CVD process, which uses flat metal substrates as template and is able to produce a low amount of graphene, 3D graphene architectures can be fabricated by using different 3D templates like nickel foam in large quantities [37].

Pioneered by Chen *et al.* [61], they reported a general strategy for the growth of graphene films directly on the 3D nickel template by decomposition of methane ( $\text{CH}_4$ ) at  $1000^\circ\text{C}$  under ambient pressure. The wrinkles present in the surface of graphene film, which is due to the difference between thermal expansion coefficients of nickel and graphene, provide better interactions of graphene films with polymers. Therefore, a layer of poly(methyl methacrylate) was easily deposited on the surface of fabricated graphene films in order to preserve the graphene network during etching the template. Lastly, nickel scaffold was etched in hydrochloric acid or iron chloride solution and then immersed in hot acetone to remove polymeric layer. Figure 11.8 shows the schematic illustration of production of 3D graphene foam by using nickel template.

It should be noted that the surface area of fabricated 3D graphene networks depends on the number of layers in the graphene film [9]. For instance, a high surface area of  $850\text{ m}^2/\text{g}$  was reported in the case of three-layer graphene foam [61]. Another important parameter is the pore size of the chosen templates since it directly affects the final properties of graphene

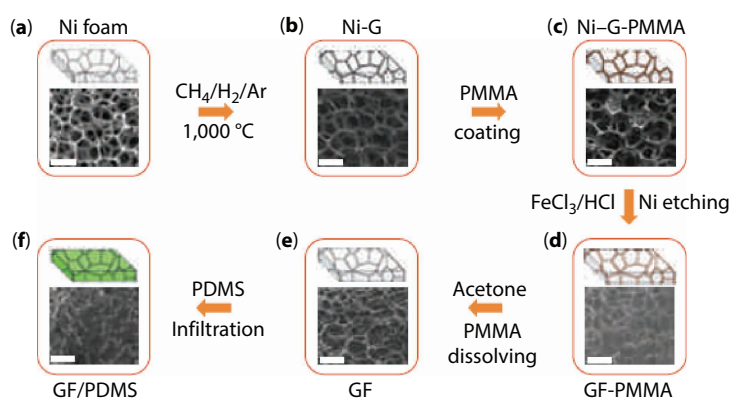


**Figure 11.8** Synthesis of 3D graphene foam (GF) and integration with poly(dimethyl siloxane) (PDMS). (a, b) CVD growth of graphene films using nickel foam as the 3D scaffold template. (c) An as-grown graphene film after coating a thin PMMA supporting layer. (d) A GF coated with PMMA after etching the nickel foam with hot HCl (or  $\text{FeCl}_3/\text{HCl}$ ) solution. (e) A free-standing GF after dissolving the PMMA layer with acetone. (f) A GF/PDMS composite after infiltration of PDMS into a GF. All the scale bars are  $500\ \mu\text{m}$  [61]. (Reproduced with permission of Springer Nature.)

foam [9]. Therefore, along with the 3D nickel foam, another template precursors have been explored. In one of the studies, 3D graphene was grown on an anodic aluminum oxide template with an average pore size of 95 nm at a temperature of 1200°C for 30 minutes under the flows of argon, hydrogen, and methane [62]. Ning *et al.* [63] demonstrated that by using a porous MgO layer as a template and methane as a carbon precursor, one to two graphene layers with an extraordinary large surface area of 1654 m<sup>2</sup>/g and an average pore size of 10 nm were formed on the surface of the template. In addition to the above-mentioned templates, the use of other templates such as metallic salts was also reported [64, 65]. Over and above this, in order to tailor the pore size of 3D graphene foam, Ito *et al.* [66] designed a novel nanoscale nickel template by electrochemically leaching manganese from a Ni<sub>30</sub>Mn<sub>70</sub> precursor in a weak acid solution. Three-dimensional graphene foam with a pore size of 100 nm to 2.0 μm was achieved by controlling the size of nickel ligaments by monitoring CVD time and temperature.

As an alternative approach, the nontemplate direct deposition of 3D graphene networks through plasma-enhanced CVD method was also reported. By using methane as carbon source and substrates like gold and stainless steel, graphene sheets were firmly adhered to the substrate and connected to each other to form 3D graphene architectures [67].

## 11.4 3D Graphene Structures

In order to enhance the functionalities and performance of the graphene-based materials in different application areas, tremendous efforts have been devoted to develop new 3D graphene-based architectures with different morphologies. In this section, a review of the most typical structures along with their characteristics has been discussed in detail.

### 11.4.1 Spheres

Graphene-based spheres, thanks to their promising properties like high electrical conductivity and large surface area, are one of the most reported 3D graphene architectures. Template-assisted method and assembly approach are the main techniques for the fabrication of graphene-based spheres [52, 68, 69]. Typically spherical templates like SiO<sub>2</sub> and PS are used to convert 2D graphene sheets to 3D graphene spheres. For example, hollow graphene/polyaniline (PANI) hybrid spheres were fabricated *via* layer-by-layer assembly of negatively charged GO sheets and positively charged PANI on the surface of sulfonated PS spheres followed by the removal of the template (Figure 11.9a) [69]. Recently, graphene nanoballs with crumpled structure were fabricated through using an aerosol-assisted capillary compression method shown in Figure 11.9b and c. To this aim, GO aqueous solution containing various metals or metal oxides (e.g., Pt and SnO<sub>2</sub>) were sprayed into a tube furnace carrying nitrogen gas at a temperature of 800°C, which led to a rapid evaporation of solvent and thus compression and aggregation of GO sheets and formation of crumpled 3D graphene balls [70]. In another novel approach, hollow and filled graphene-based spheres was fabricated through one-step core-shell electro spraying technique without applying any post-treatment or using any template (Figure 11.9d, e) [8]. Using precursor-assisted CVD technique, Lee *et al.* synthesized mesoporous graphene nanoballs in which iron chloride

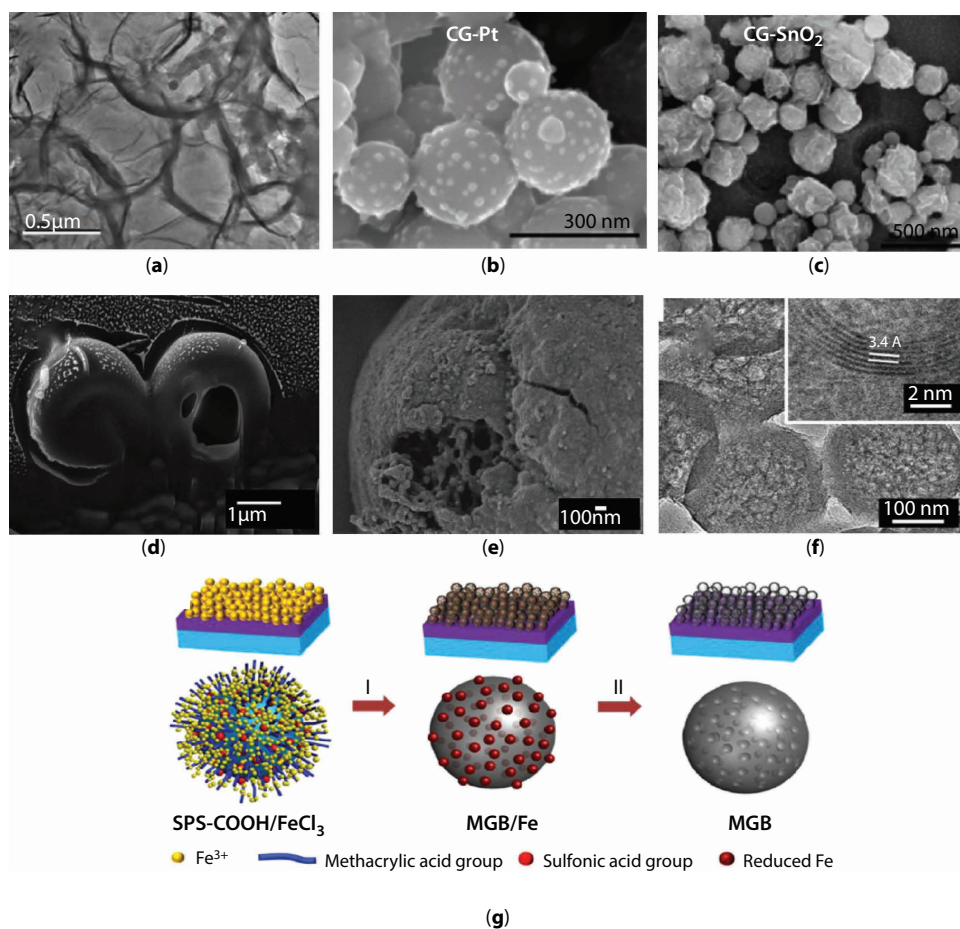


**Figure 11.9** (a) TEM image of rGO/PANI hollow spheres *via* layer-by-layer assembly method [69]. (Reproduced with permission of Elsevier.) (b, c) SEM images of crumpled graphene balls composites synthesized by direct aerosolization of a GO suspension mixed with precursor ions: graphene balls composited with  $\text{SnO}_2$  (a) and Pt (b) [70]. (Reproduced with permission of American Chemical Society.) (d) FIB-SEM image of core-shell electrospayed hollow graphene-based PMMA spheres. (e) SEM image of core-shell electrospayed filled graphene-based PS spheres [8]. (Reproduced with permission of Royal Society of Chemistry.) (f) High-resolution TEM image of mesoporous graphene nanoballs obtained by CVD with an interlayer spacing of 0.34 nm. (g) The fabrication process of mesoporous graphene nanoballs: step 1, drop casting of the SPS-COOH/ $\text{FeCl}_3$  solution onto the substrate and subsequent CVD growth of graphene; step 2, the removal of iron domains to leave the nanoballs [71]. (Reproduced with permission of American Chemical Society.)

and PS balls were used as the catalyst precursor and carbon source, respectively. Obtained graphene nanoballs, which are given in Figure 11.9f, showed a large specific surface area of  $508 \text{ m}^2/\text{g}$ . Figure 11.9g illustrates the schematic representation of produced mesoporous nanoballs, where PS balls were first functionalized with carboxylic acid and sulfonic acid groups in order to enhance the dispersion of PS balls in  $\text{FeCl}_3$  solution and then annealed at  $1000^\circ\text{C}$  under hydrogen atmosphere. During the process, the adsorbed iron ions on the surface of PS were reduced to iron metals, and thus it acted as 3D domains and catalyst for the growth of graphene through CVD method [71].

### 11.4.2 Networks

Three-dimensional graphene networks, including graphene foams [72, 73], hydrogels [74, 75], aerogels [76, 77], and sponges [78, 79], are the most reported 3D graphene architectures. CVD technique is the main method for the production of high-quality 3D graphene networks where few layers of graphene are deposited on the surface of a metal substrate through carbon dissolution and segregation mechanism. Figure 11.10a–d represents the CVD grown-graphene networks before and after etching the template [80]. Obtained 3D graphene networks contain less defects than chemically derived graphene, which can be also approved by Raman characterization technique [61, 80]. Since D-band ( $\sim 1350\text{ cm}^{-1}$ ), a characteristic peak in the Raman spectra of graphene, is related to disorderness and its intensity changes with the defects in the structure [81], disappearance of D band of CVD growth graphene network in the Raman spectra confirms the formation of defect-free graphene (Figure 11.10f).

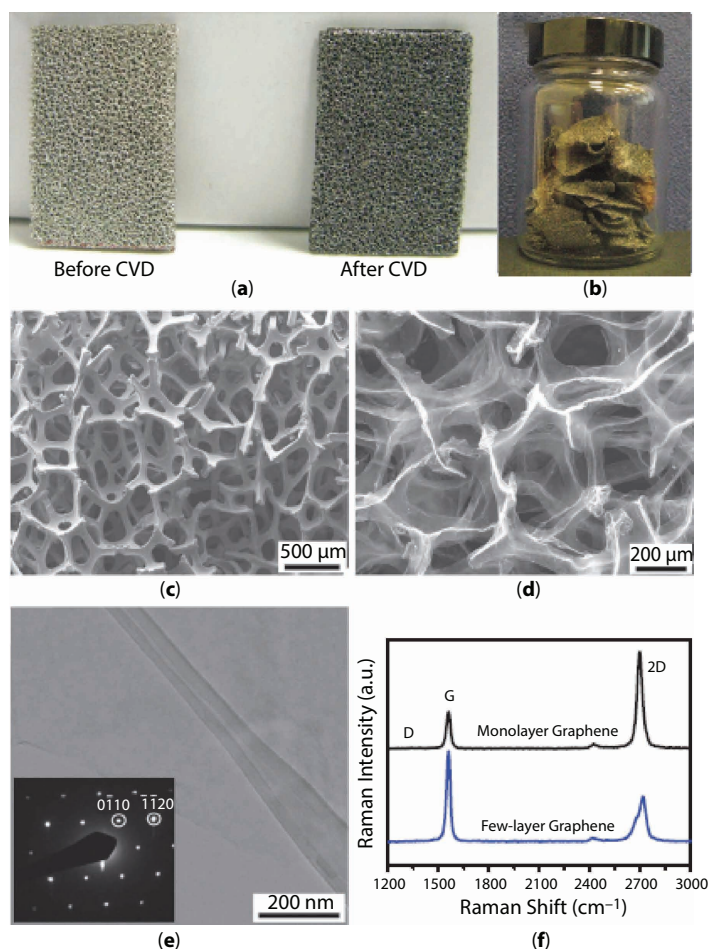


**Figure 11.10** Photographs of (a) Ni foam before and after the growth of graphene, and (b)  $\approx 0.1\text{ g}$  3D graphene networks obtained in a single CVD process after removal of the Ni foam. SEM images of (c) 3D graphene networks grown on Ni foam after CVD, and (d) 3D graphene networks after removal of Ni foam. (e) TEM image of a graphene sheet. Inset: SAED pattern of graphene sheet. (f) Raman spectra of 3D graphene networks [80]. (Reproduced with permission of Wiley.)

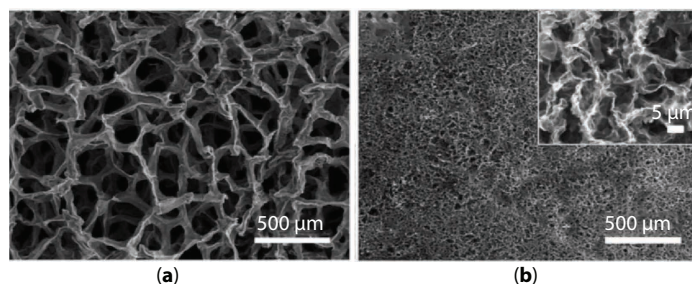


**Figure 11.11** Comparison of 3D graphene networks obtained by using two different templates of (a) commercial nickel foam and (b) cross-linked nickel skeleton [82]. (Reproduced with permission of Springer Nature.)

Despite their high quality, CVD growth graphene networks suffer from large pore sizes (e.g., hundreds of micrometers), high porosity (e.g., ~99.7%), and thus low yield [61]. To address this problem, many studies have been focused on using different templates. In one of the works, Lee *et al.* [82] reported the fabrication of high-density 3D graphene networks by using nickel chloride hexahydrate as catalyst precursor by annealing it at 600°C. After annealing, 3D graphene foam was grown at the different temperatures on the cross-linked nickel skeleton in the presence of hydrogen and argon atmosphere. Figure 11.11a and b shows the difference between CVD growth 3D graphene networks with commercial nickel template and cross-linked nickel skeleton. The pore size of 3D graphene networks grown from commercial nickel template was one to two orders of magnitude greater than the one grown with cross-linked nickel template. As a consequence, the smaller pore size of annealed template led to the relatively higher density of 3D graphene networks ranging from 22 to 100 mg/cm<sup>3</sup>, compared with that of the nickel foam (1 mg/cm<sup>3</sup>).

The effect of growth temperature on the structure of 3D graphene networks was investigated by Raman spectroscopy (Figure 11.12a, b). Lee *et al.* [82] demonstrated that the quality of 3D graphene networks was improved by increasing the growth temperature up to 1000°C since defects in the structure decreased and thinner graphene layers were formed as D-band (~1340 cm<sup>-1</sup>) disappeared and the intensity of 2D-band (~2750 cm<sup>-1</sup>) increased, respectively (Figure 11.12a). In the Raman spectra of graphene, the intensity ratio of 2D-band to G-band (~1575 cm<sup>-1</sup>) together with the 2D-band full-width at half maximum estimate the number of graphene layers (Figure 11.12b) [81]. The existence of monolayer, bilayer, and multilayer graphene at the same time in the structure was attributed to the various sizes of cross-linked nickel grains in the template (Figure 11.12f–k).

In addition to CVD, 3D graphene networks could be synthesized through different approaches such as assembly methods [47, 83] and template-assisted technique [84].

### 11.4.3 Films

In the past few years, many efforts have been devoted on the fabrication of 3D graphene films since it possesses large surface area, interconnected framework, and good mechanical strength, which make it an ideal candidate for many applications especially energy-related areas. However,  $\pi$ - $\pi$  interactions and van der Waals forces between 2D graphene sheets cause

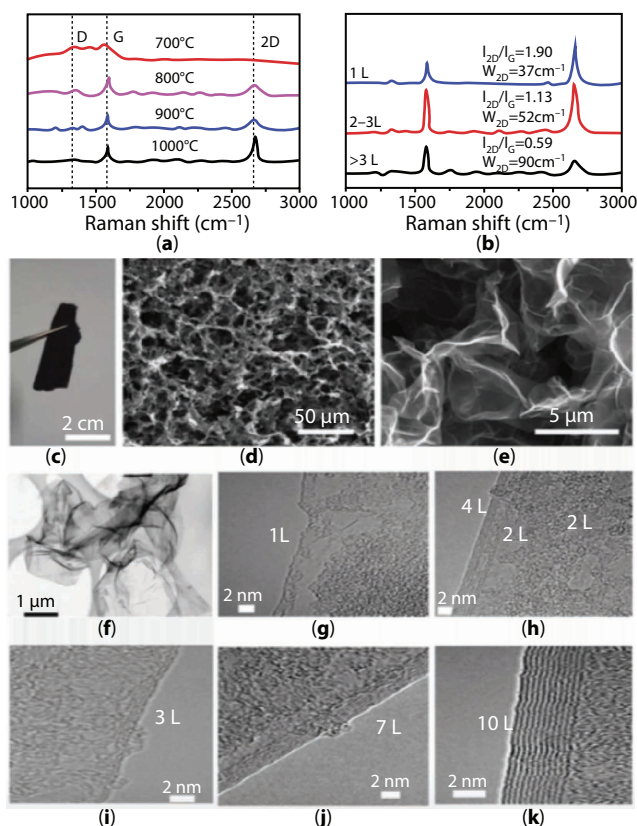


**Figure 11.12** (a) Typical Raman spectra of 3D graphene network grown with different temperatures for 1.5 min. The Raman spectra show that the quality of 3D graphene networks is gradually improved with increasing the growth temperature up to 1000°C. (b) Typical Raman spectra of a 3D graphene network. Multilayer, bilayer, and monolayer graphene from bottom to top estimated by the intensity ratio of 2D peak to G peak, combining with 2D-band full-width at half maximum (FWHM,  $W_{2D}$ ). (c) A photograph of the free-standing 3D graphene network. (d, e) SEM images of honeycomb-like graphene layers after etching nickel template with FeCl<sub>3</sub>/HCl solution at different magnifications. (f) Low-resolution TEM image of the graphene layers in 3D graphene network. (g–k) High-resolution TEM images of different graphene layers in 3D graphene network. (g) Monolayer. (h) Double layers and four layers. (i) Three layers. (j) Seven layers. (k) Ten layers [82]. (Reproduced with permission of Springer Nature.)

a significant loss in the surface area and thus limit the usage of graphene films in practical applications [37, 85]. For understanding the behavior of graphene sheets in bulky structure, one can consider graphite as a packed case of graphene, although it lacks many of the superior characteristics of single sheet graphene as a consequence of dense packing [86]. To address this problem, further consideration such as addition of spacer materials is essential to inhibit intersheet restacking of sheets. Up to now, the incorporation of spacer materials such as polymers [87], noble metals [88], metal oxides and hydroxides [89, 90], carbon materials [91], and metal organic frameworks [92] in between the 2D graphene sheets has been reported. In addition to the above-mentioned materials, different templates (e.g., PS, PMMA, and SiO<sub>2</sub> spherical particles) could be used to prevent the agglomeration problem of graphene sheets. Choi *et al.* [93] prepared MnO<sub>2</sub> deposited 3D macroporous graphene frameworks by using

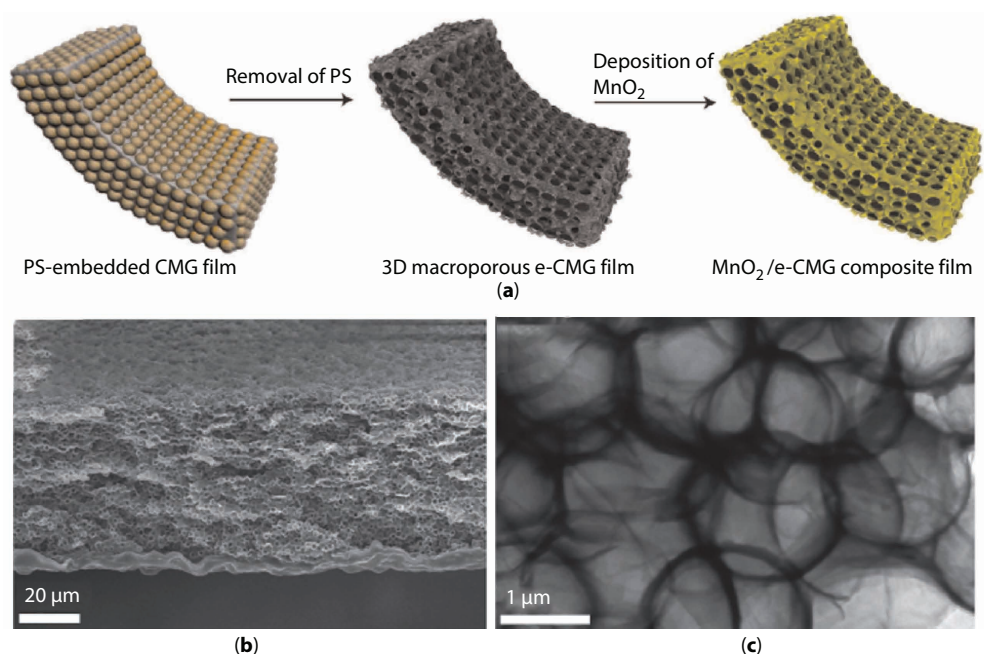


**Figure 11.13** (a) Schematic illustration of the fabrication procedure of 3D macroporous  $\text{MnO}_2$ -chemically modified graphene films, (b) SEM, and (c) TEM images of the chemically modified graphene films [93]. (Reproduced with permission of American Chemical Society.)

PS spherical particles as a template followed by the filtration and removal of the template (Figure 11.13). The proposed material exhibited high electrical conductivity and surface area, which makes it a great potential as electrode material for supercapacitors.

In another study, Yang *et al.* [86] by inspiration from nature demonstrated that the water molecules can act as a natural spacer for enlarging the space in between the graphene sheets and inhibit the agglomeration. So the resultant graphene film could act as a high-performance electrode material since water molecules provided a porous structure, allowing the electrolyte ions to access the inner surface area of each sheet individually. Interestingly, although the obtained film contained almost 92 wt% water, it showed a high electrical conductivity, which might stem from face-to-face-stacked morphology of the wet film and provided electron transport paths in the structure.

At the same time, some different methods like tape casting [94], leavening [95], light scribing [96], and chemical activation [97] have been developed for the fabrication of porous graphene films without using spacer materials.

#### 11.4.4 Other Novel Architectures

In addition to the aforementioned 3D graphene architectures, the fabrication of different structures like 3D graphene scrolls [98], tubes [99], and honeycombs [100] have also been reported. Figure 11.14 represents some of 3D graphene structures, which are reported in the literature. In a work reported by Zhang *et al.* [98], nitrogen-doped graphene ribbon assembled core–sheath  $\text{MnO}@$ graphene scrolls was fabricated by a combination of

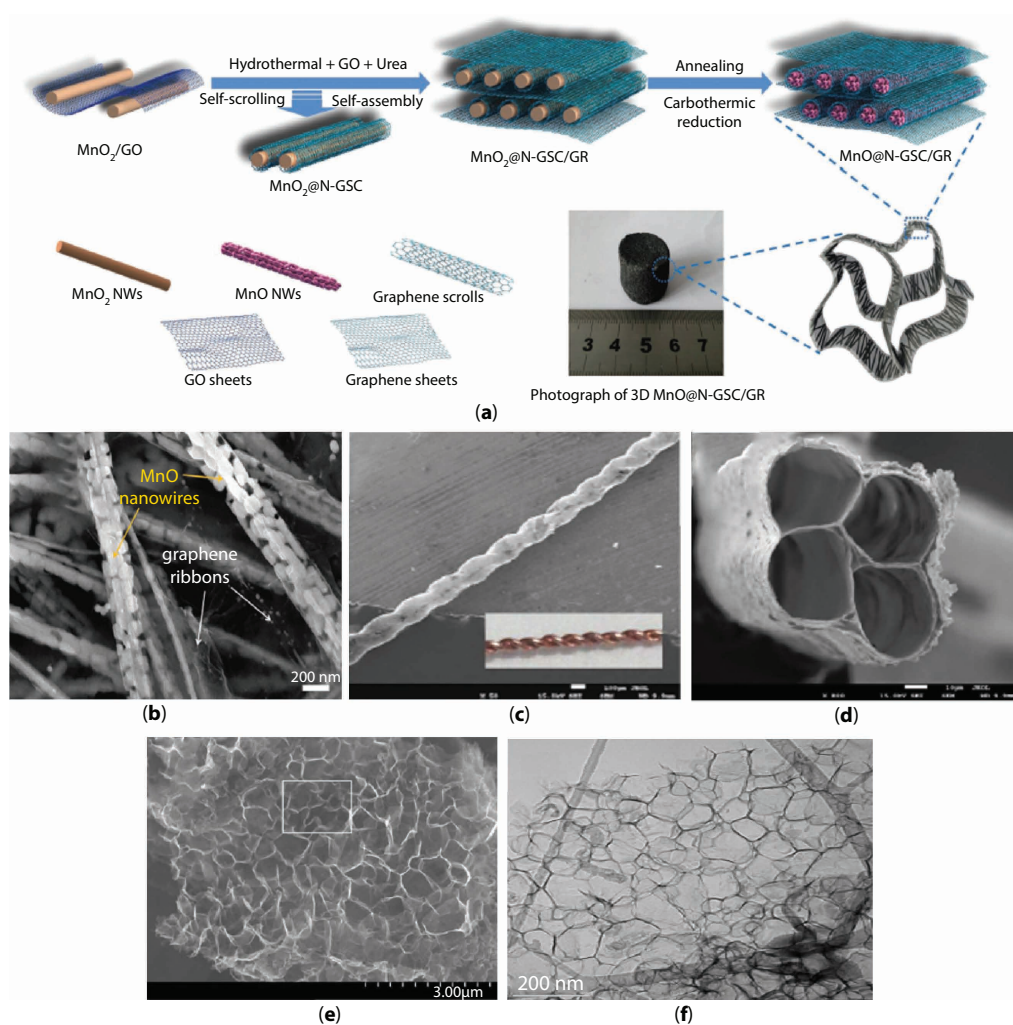


**Figure 11.14** (a) Schematic representation of the fabrication process for the 3D hierarchical MnO@N-doped graphene scrolls/graphene ribbons architecture, involving two main steps of the self-scrolling and self-assembly process between MnO<sub>2</sub> nanowires and GO sheets as well as a subsequent annealing treatment. (b) FESEM images of MnO@N-doped graphene scrolls/graphene ribbons at different magnifications [98]. (Reproduced with permission of Wiley.) (c) SEM image of helical graphene microtubings made by using a twist of two Cu wires of 100 μm in diameter (inset). (d) SEM image of the multichannel graphene microtubings with a channel number of 4 (the used Cu wire is 40 μm in diameter) Scale bars: c, 100 μm; d, 10 μm [99]. (Reproduced with permission of American Chemical Society.) (e) High-angle annular dark field image and (f) TEM image of a honeycomb-structured graphene [101]. (Reproduced with permission of Wiley.)

hydrothermally assisted self-assembly and an N-doping strategy (Figure 11.14a, b). The obtained 3D architecture could serve as a high-performance electrode in lithium storage devices.

In another study, 3D graphene microtubings were prepared through hydrothermal method and Cu wires as template. The morphology of graphene-based tubes is similar to that of CNTs, although the inner diameter of tubes is much larger when compared to CNT.

In this work, Cu wires were placed inside a glass pipeline and then GO dispersion was filled in the pipeline. During hydrothermal reduction, GO sheets were wrapped around the Cu wires and 3D graphene microtubings were obtained by removing the template and pipeline (Figure 11.14c, d) [99].

Honeycomb-like 3D graphene architecture was fabricated by a simple reaction of lithium oxide and carbon monoxide gas under low pressure at 550°C, which is shown in Figure 11.14e and f. The obtained structure exhibited a high-energy conversion efficiency, which makes it a promising material in the energy storage devices [101].

## 11.5 Applications of 3D Graphene Architectures

As discussed above, 3D graphene structures with improved performance and advanced functionalities compared to 2D graphene sheets have been widely used in many applications such as energy storage devices, sensors, polymeric composites, and catalysis.

### 11.5.1 Supercapacitors

Supercapacitors have drawn significant attention compared to other energy-storage devices owing to their advanced properties like high power density and long cycle life [102]. Based on energy-storing mechanisms, supercapacitors divide into two main groups, which are pseudo-capacitors and electrochemical double-layer capacitors (EDLCs). Pseudo-capacitors like transition metal oxides and conducting polymers store the charges *via* chemical redox reaction on the surface, whereas EDLCs (e.g., carbon-based materials) store the energy by ion adsorption on the electrode–electrolyte surface. Among various carbon-based materials, graphene as an EDLC electrode is widely used in the electrochemical energy storage systems owing to its rich variety of dimensionality and large surface area [103]. Very recently, 3D graphene structures became an attractive candidate for supercapacitors thanks to their porous structure, high surface area, and interconnected network, which improves the accessibility of electrolyte ions to the surface of electrode and increases the electrical conductivity [104]. So far, different structures of 3D graphene-based materials like spheres [49], networks [80], and films [105] have been reported as potential electrodes for supercapacitors. In the following, the supercapacitor applications of the reported graphene structures and their related composites have been discussed in detail.

Graphene spheres with hollow micro/nanostructures offer advanced characteristics such as high surface area and shortened diffusion length for charge and mass transport, which can greatly enhance the performance as electrode for supercapacitor [106]. For instance, graphene-wrapped polyaniline hollow spheres were fabricated by deposition of PANI polymer on the sulfonated PS spherical templates followed by the removal of template to obtain hollow PANI spheres. Then negatively charged GO sheets were wrapped on the positively charged PANI hollow spheres *via* electrostatic interaction and then were reduced to graphene through electrochemical reduction (Figure 11.15a, b). Obtained graphene-wrapped polyaniline hollow spheres exhibited an excellent specific capacitance of 614 F/g at a current density of 1 A/g and over 90% retention of the capacitance after 500 charging–discharging cycles (Figure 11.15c, d) [107]. In another work reported by Lee *et al.* [71], mesoporous

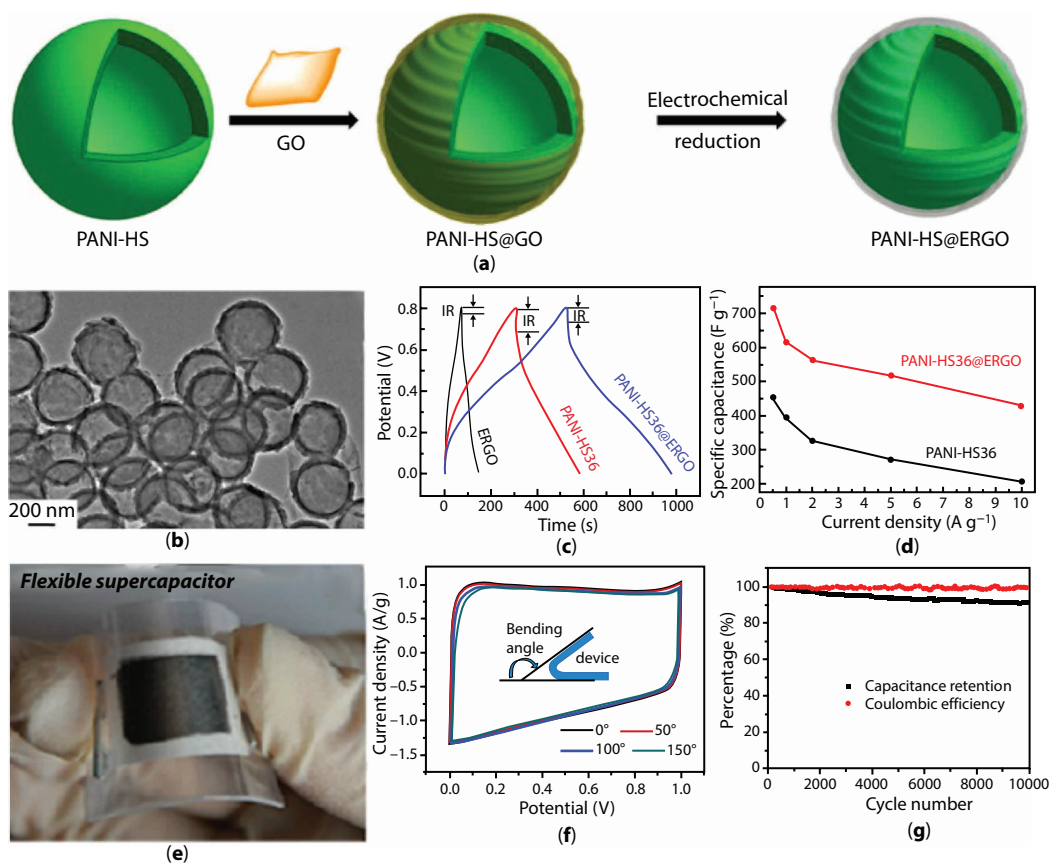


**Figure 11.15** (a) Schematic illustration of the preparation steps, and (b) TEM image of graphene-wrapped hollow PANI spheres. (c) Galvanostatic charge–discharge curves of electrochemically reduced GO, PANI hollow spheres, and graphene-wrapped PANI hollow spheres within a potential window of 0–0.80 V at a current density of 1 A/g. (d) Plots of specific capacitance for PANI hollow spheres and graphene-wrapped PANI hollow spheres at various current densities [107]. (Reproduced with permission of American Chemical Society.) (e) Digital photograph of 3D graphene/MnO<sub>2</sub> composite networks as flexible supercapacitor [110]. (Reproduced with permission of American Chemical Society.) (f) CV curves of the flexible solid-state supercapacitor based on the 3D graphene hydrogels at 10 mV/s for different bending angles. (g) Cycling stability of the flexible solid-state supercapacitor based on the 3D graphene hydrogels at a current density of 10 A/g [109]. (Reproduced with permission of American Chemical Society.)

graphene nanoballs as electrode for supercapacitors were prepared by using CVD method and showed high specific capacitance of 206 F/g at a scan rate of 5 mV/s. After 10,000 cycles of charging–discharging, even at high current density, mesoporous graphene nanoballs still exhibited 96% retention of capacitance.

Three-dimensional graphene networks like graphene foam, sponges, and hydrogels have attracted great attention due to their desired porous structure, which enhances the movement of electrolyte ions inside the graphene frameworks and thus increases the electrical conductivity and electrochemical performance of the electrode materials [45]. Sponge-like graphene nanoarchitectures fabricated by microwave synthesis of graphene and CNT exhibited a high energy density of 7.1 W·h/kg at an extra high power density of 48,000 W/kg

and retention of 98% after 10,000 cycles of charging–discharging in 1 M sulfuric acid as electrolyte. The high performance of the obtained structure may be attributed to the large surface area of 418 m<sup>2</sup>/g and fully accessible porous network [78].

Up to now, considerable efforts have been dedicated for the fabrication of flexible supercapacitors as the potential power supplies for future wearable and portable devices like electronic textiles [108]. Concerning this, Xu *et al.* [109] produced a flexible solid-state supercapacitor from graphene hydrogel film as electrode and polyvinyl alcohol and sulfuric acid as electrolyte. The obtained electrode with a thickness of 120 μm showed a high gravimetric capacitance of 186 F/g at a current density of 1 A/g and excellent cycling capability of 91.6% retention after 10,000 charge–discharge cycles (Figure 11.15f, g). Besides, 3D graphene hydrogel films with interconnected networks presented high electrical and mechanical robustness, which is essential for the flexible supercapacitor applications. Recently, He *et al.* [110] presented an ultralight and freestanding flexible supercapacitor of graphene/MnO<sub>2</sub> composite networks, shown in Figure 11.15e, *via* CVD growth of graphene on the nickel foam subsequently followed by electrochemical deposition of MnO<sub>2</sub> on the 3D graphene network. A high specific capacitance of 130 F/g at a scan rate of 2 mV/s and low resistance variations upon bending up to 180° were achieved, which confirms the excellent electrochemical performance of the obtained 3D graphene networks.

### 11.5.2 Lithium-Ion Batteries

In recent years, 3D graphene structures have been extensively studied for their potential use as active electrodes in batteries. The integration of 3D graphene into the structure of electrodes improves the lifetime and energy density as well as the electrochemical performance of the electrodes since the batteries usually suffer from low reversible capacity and cyclic life when compared to supercapacitors. Therefore, in the design of batteries (e.g., lithium-ion batteries, LIBs), one should consider the importance of the LIB components (e.g., electrodes and electrolytes) role in the improvement of the battery performance. By virtue of outstanding characteristics like high surface area, porous structure, fast mass/charge transfer, and interconnected network, 3D graphene architectures became an outstanding candidate for high-performance LIBs.

So far the incorporation of various metal or metal oxides (e.g., Sn [111], NiO [112], Fe<sub>3</sub>O<sub>4</sub> [113], LiFePO<sub>4</sub> [114]) and CNT [115] with graphene sheets and fabrication of 3D graphene composites have been studied. Yu and co-workers [116] developed mesoporous TiO<sub>2</sub> spheres embedded in 3D graphene networks by a facile hydrothermal self-assembly strategy. The as-prepared composite as a negative electrode for LIBs exhibited an excellent high-rate capacitance of 124 mA h/g at a current rate of 20 C when compared to that of pure TiO<sub>2</sub> as 38 mA h/g (Figure 11.16a, b). Such an improvement in the electrochemical performance of the as-prepared composite may be attributed to the high contact area between the electrolyte and electrode, desired diffusion kinetics for both electrons and lithium ions, and high electrical conductivity of the 3D graphene networks as well as porous structure of TiO<sub>2</sub> spheres.

Using microwave-assisted synthesis of self-assembled 3D graphene/CNT/Ni, Bae *et al.* [115] developed a new electrode for LIBs in which CNTs were grown on graphene sheets through tip growth mechanism by Ni nanoparticles and acted as a spacer by preventing

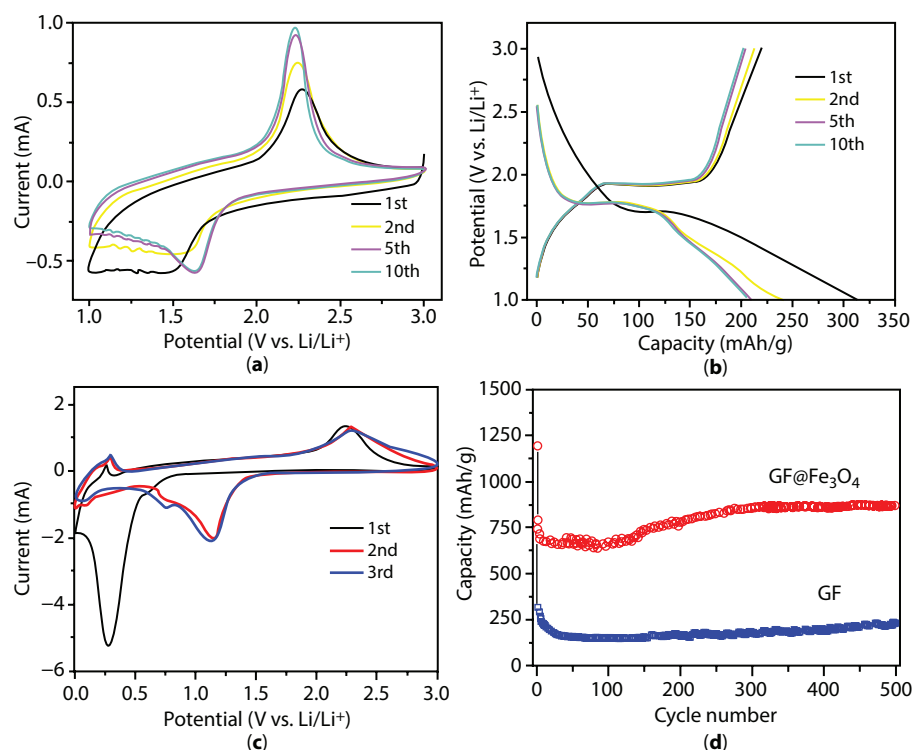


**Figure 11.16** (a) Representative cyclic voltammograms of the TiO<sub>2</sub> spheres embedded in 3D graphene networks at a scan rate of 1 mV/s. (b) Charge-discharge voltage profiles of the TiO<sub>2</sub> spheres embedded in 3D graphene composite at a current rate of 0.5 C [116]. (Reproduced with permission of Royal Society of Chemistry.) (c) CV curves of the graphene foam supported Fe<sub>3</sub>O<sub>4</sub> electrode. (d) Cycling profiles of the graphene foam and graphene foam supported Fe<sub>3</sub>O<sub>4</sub> electrodes at 1-C rate [113]. (Reproduced with permission of American Chemical Society.)

the re-stacking of 2D graphene sheets. The synthesized 3D composite as anode electrode for LIBs showed a reversible specific capacity of 648.2 mA h/g after 50 cycles at a current density of 100 mA/g.

Due to its high theoretical capacity, low cost, and nontoxic properties, Fe<sub>3</sub>O<sub>4</sub> has been considered as a promising electrode for LIBs. However, high volume expansion and the low conductivity of Fe<sub>3</sub>O<sub>4</sub> prohibit stable performance of electrodes. Integration of conductive nanomaterials like graphene and construct 3D architectures is one of the main strategies to improve the performance of Fe<sub>3</sub>O<sub>4</sub>-based electrodes. To this aim, Luo *et al.* [113] prepared 3D graphene foam supported Fe<sub>3</sub>O<sub>4</sub> LIB, which exhibited a high capacity of 785 mA h/g at 1 C charge-discharge rate without decay up to 500 cycles. The electrochemical properties of the graphene-supported Fe<sub>3</sub>O<sub>4</sub> LIB electrodes are given in Figure 11.16c and d.

In all of the above-mentioned studies, 3D graphene provides a short path length for Li ion as well as electron transport and increases the conductivity by eliminating the agglomeration and thus improves the electrode performance.

### 11.5.3 Sensors

In recent years, graphene-based materials decorated with metals and metal oxides have been studied in various sensing devices (e.g., electrochemical sensing and bio-sensing) due to graphene's excellent optoelectronic properties as well as high catalytic activity of the metals/metal oxides [117]. For example, Yavari *et al.* [118] prepared a 3D graphene network for the detection of  $\text{NH}_3$  and  $\text{NO}_2$  at room temperature and atmospheric pressure with a high sensitivity of gas detection in the ppm range. In another study, Kung *et al.* [119] designed a platinum–ruthenium bimetallic nanocatalyst integrated 3D graphene foam as a sensor for the detection of hydrogen peroxide by enhancing the surface area and improving the effective transport in the reaction. The proposed material exhibited high performance toward electrochemical oxidation of  $\text{H}_2\text{O}_2$  with a high sensitivity of  $1023.1 \mu\text{A}/\text{mM cm}^2$  and low detection limit of 0.04 mM.

Large-area 3D graphene interconnected GO intercalated by PANI nanofibers for the determination of guanine and adenine have been constructed by Yang *et al.* [120]. By the help of strong  $\pi$ – $\pi$  interactions and electrostatic adsorption, positively charged guanine and adenine adsorbed to the negatively charged proposed structure. High sensitivity, long-term stability, and low detection limit of the prepared material make it a reliable approach for the determination of other small molecules.

### 11.5.4 Fuel Cells

Nowadays, the finite nature of fossil fuels and rapid increase in energy consumption persuade the scientists to design and develop renewable energy sources. To this aim, 3D graphene architectures have attracted great attention in the fuel cells as catalysts or catalyst carrier supporting metals and alloys in oxidation and oxygen reduction reactions (ORR) and thus improve the performance of the fuel cell [45]. Microbial fuel cells (MFCs) convert the chemical energy in biodegradable organic materials into electricity *via* bio-oxidation process and thus provide environmental bioremediation. However, most of the commercially available MFCs suffer from low power density and low bacteria loading on the surface of the electrodes. To address this problem, many studies have focused on the integration of catalysts materials to both anode and cathode of the MFCs [121, 122]. Very recently, the use of 3D graphene as catalysts or support material has gained great attention because of the large surface area and high electrical conductivity of 3D graphene structures. In one of the studies, Yong *et al.* [122] suggested a macroporous and monolithic anode electrode based on PANI hybridized 3D graphene. Owing to large surface area of graphene, the ability of integration with bacterial films has improved and thus more electrons passed through multiplexing and conductive pathways. The schematic illustration of the interface and interactions between 3D graphene/PANI electrode and bacteria is shown in Figure 11.17a. As shown in Figure 11.17b and c, obtained MFC exhibited a high power density of  $768 \text{ mW}/\text{m}^2$ , which is four times higher than that of the carbon cloth MFC under the same conditions. Similarly, 3D graphene aerogel decorated with Pt nanoparticles has been fabricated as a freestanding anode for MFCs with an excellent power density of  $1460 \text{ mW}/\text{m}^2$ . The superior performance of prepared MFC was attributed to the high bacteria loading capacity, easy electron transfer between the bacteria and the 3D graphene/Pt, as well as fast ion diffusion in 3D pores [123].

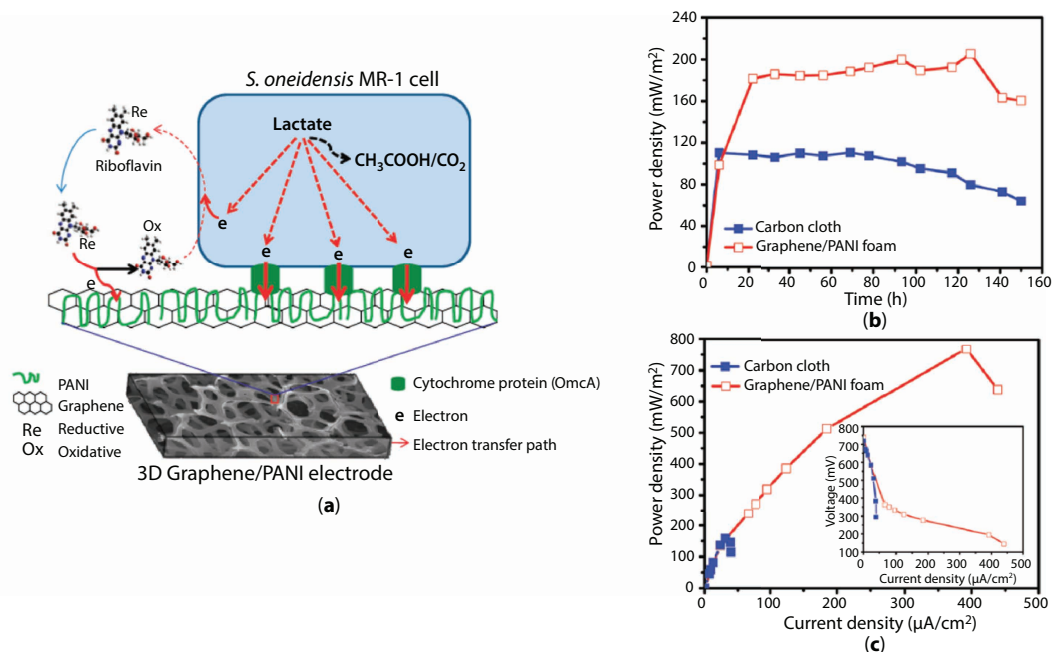


**Figure 11.17** (a) Schematic illustration of the interface between 3D graphene/PANI monolith electrode and *S. oneidensis* MR-1 bacteria. (b) Time courses of the power density output of the MFCs equipped with a carbon cloth anode or a graphene/PANI foam anode. (c) Polarization curves of the two types of MFCs. The inset shows the I–V relation [122]. (Reproduced with permission of American Chemical Society.)

## 11.6 Conclusions and Perspectives

This review summarized the recent developments in 3D graphene-based materials by tailoring morphologies based on their characteristics and applications. So far, considerable efforts have been devoted to the design and fabrication of 3D graphene materials in the form of spheres, films, and networks. Three-dimensional graphene not only preserves the intrinsic properties of 2D graphene by inhibiting the re-stacking and aggregation of sheets, but also provides advanced functionalities with desired characteristics in various applications such as supercapacitors, fuel cells, batteries, sensors, etc. The main approaches for the construction of 3D graphene architectures are assembly method, template-assisted techniques, chemical vapor deposition, and electrospinning technology. Nevertheless, there are still some challenges in the production of the 3D graphene architectures. For instance, the size of constructed structures and their properties strongly depend on the building blocks (e.g., templates). Besides, the main problem of graphene sheets is their tendency to agglomeration, which strongly decreases the electrical conductivity and utilization of graphene in bulk applications. So there is still a need to design new and feasible approaches that can prevent the re-stacking of graphene layers and fabricate an ideal 3D graphene structure and convey the production scale from laboratory to pilot scale by lowering the costs. Finally, 3D graphene structures bring new opportunities in the commercialization of graphene-based products and open up new opportunities in energy, electronic, and composite applications.

## References

1. Du, X., Skachko, I., Barker, A., Andrei, E.Y., Approaching ballistic transport in suspended graphene. *Nat. Nanotechnol.*, 3, 8, 491–495, 2008.
2. Balandin, A.A., Ghosh, S., Bao, W., Calizo, I., Teweldebrhan, D., Miao, F., Lau, C.N., Superior thermal conductivity of single-layer graphene. *Nano Lett.*, 8, 3, 902–907, 2008.
3. Zhu, Y., Murali, S., Cai, W., Li, X., Suk, J.W., Potts, J.R., Ruoff, R.S., Graphene and graphene oxide: Synthesis, properties, and applications. *Adv. Mater.*, 22, 35, 3906–3924, 2010.
4. Galashev, A.E. and Rakhmanova, O.R., Mechanical and thermal stability of graphene and graphene-based materials. *Physics-Uspokhi*, 57, 10, 970–989, 2014.
5. Lee, C., Wei, X., Kysar, J.W., Hone, J., Measurement of the elastic properties and intrinsic strength of monolayer graphene. *Science (80)*, 321, 5887, 385–388, 2008.
6. Mao, S., Lu, G., Chen, J., Three-dimensional graphene-based composites for energy applications. *Nanoscale*, 2014.
7. Zhao, Y., Jiang, C., Hu, C., Dong, Z., Xue, J., Meng, Y., Zheng, N., Chen, P., Qu, L., Large-scale spinning assembly of neat, morphology-defined, graphene-based hollow fibers. *ACS Nano*, 7, 3, 2406–2412, 2013.
8. Haghghi Poudeh, L., Saner Okan, B., Seyyed Monfared Zanjani, J., Yildiz, M., Menceloglu, Y.Z., Design and fabrication of hollow and filled graphene-based polymeric spheres *via* core-shell electrospinning. *RSC Adv.*, 5, 91147–91157, 2015.
9. Bagoole, O., Rahman, M., Younes, H., Shah, S., Al Ghaferi, A., Three-dimensional graphene interconnected structure, fabrication methods and applications: Review. *J. Nanomed. Nanotechnol.*, 8, 2, 2017.
10. Novoselov, K.S., Geim, A.K., Morozov, S.V., Jiang, D., Zhang, Y., Dubonos, S.V., Grigorieva, I.V., Firsov, A.A., Electric field effect in atomically thin carbon films. *Science (80)*, 306, 5696, 666–669, 2004.
11. Sutter, P.W., Flege, J.-I., Sutter, E.A., Epitaxial graphene on ruthenium. *Nat. Mater.*, 7, 5, 406–411, 2008.
12. Kim, K.S., Zhao, Y., Jang, H., Lee, S.Y., Kim, J.M., Kim, K.S., Ahn, J.-H., Kim, P., Choi, J.-Y., Hong, B.H., Large-scale pattern growth of graphene films for stretchable transparent electrodes. *Nature*, 457, 7230, 706–710, 2009.
13. Lu, J., Yang, J., Wang, J., Lim, A., Wang, S., Loh, K.P., One-pot synthesis of fluorescent carbon nanoribbons, nanoparticles, and graphene by the exfoliation of graphite in ionic liquids. *ACS Nano*, 3, 8, 2367–2375, 2009.
14. Stankovich, S., Dikin, D.A., Piner, R.D., Kohlhaas, K.A., Kleinhammes, A., Jia, Y., Wu, Y., Nguyen, S.T., Ruoff, R.S., Synthesis of graphene-based nanosheets *via* chemical reduction of exfoliated graphite oxide. *Carbon N. Y.*, 45, 1558–1565, 2007.
15. Park, S. and Ruoff, R.S., Chemical methods for the production of graphenes. *Nat. Nanotechnol.*, 4, march, 217–224, 2009.
16. Li, C. and Shi, G., Three-dimensional graphene architectures. *Nanoscale*, 4, 18, 5549, 2012.
17. Dreyer, D.R., Park, S., Bielawski, C.W., Ruoff, R.S., The chemistry of graphene oxide. *Chem. Soc. Rev.*, 39, 1, 228–240, 2010.
18. Khan, M., Tahir, M.N., Adil, S.F., Khan, H.U., Siddiqui, M.R.H., Al-warthan, A.A., Tremel, W., Graphene based metal and metal oxide nanocomposites: Synthesis, properties and their applications. *J. Mater. Chem. A*, 3, 37, 18753–18808, 2015.
19. Brodie, B.C., On the atomic weight of graphite. *Phil. Trans. R. Soc. Lond.*, 149, January, 249–259, 1859.
20. Staudenmaier, L., Verfahren zur Darstellung der Graphitsaure. *Ber. Dtsch. Chem. Ges.*, 31, 1481–1487, 1898.

21. William, J., Hummers, S., Offeman, R.E., Preparation of graphitic oxide. *J. Am. Chem. Soc.*, 80, 1937, 1339, 1958.
22. Chen, J., Yao, B., Li, C., Shi, G., An improved Hummers method for eco-friendly synthesis of graphene oxide. *Carbon N. Y.*, 64, 1, 225–229, 2013.
23. Marcano, D.C., Kosynkin, D.V., Berlin, J.M., Sinitskii, A., Sun, Z., Slesarev, A., Alemany, L.B., Lu, W., Tour, J.M., Improved synthesis of graphene oxide. *ACS Nano*, 4, 8, 4806–4814, 2010.
24. Saner, B., Okyay, F., Yürüm, Y., Utilization of multiple graphene layers in fuel cells. 1. An improved technique for the exfoliation of graphene-based nanosheets from graphite. *Fuel*, 89, 8, 1903–1910, 2010.
25. McAllister, M.J., Li, J.-L., Adamson, D.H., Schniepp, H.C., Abdala, A.A., Liu, J., Herrera-Alonso, M., Milius, D.L., Car, R., Prud'homme, R.K., Aksay, I.A., Single sheet functionalized graphene by oxidation and thermal expansion of graphite. *Chem. Mater.*, 19, 18, 4396–4404, 2007.
26. Stankovich, S., Dikin, D.A., Piner, R.D., Kohlhaas, K.A., Kleinhammes, A., Jia, Y., Wu, Y., Nguyen, S.T., Ruoff, R.S., Synthesis of graphene-based nanosheets *via* chemical reduction of exfoliated graphite oxide. *Carbon N. Y.*, 45, 7, 1558–1565, 2007.
27. Saner, B., Dinç, F., Yürüm, Y., Utilization of multiple graphene nanosheets in fuel cells: 2. the effect of oxidation process on the characteristics of graphene nanosheets. *Fuel*, 90, 8, 2609–2616, 2011.
28. Si, Y. and Samulski, E.T., Synthesis of water soluble graphene. *Nano Lett.*, 8, 1679–82, 2008.
29. Xu, Y., Sheng, K., Li, C., Shi, G., Self-assembled graphene hydrogel *via* a one-step hydrothermal process. *ACS Nano*, 4, 7, 4324–4330, 2010.
30. Kim, J., Cote, L.J., Kim, F., Yuan, W., Shull, K.R., Huang, J., Graphene oxide sheets at interfaces. *J. Am. Chem. Soc.*, 132, 23, 8180–8186, 2010.
31. Bai, H., Li, C., Wang, X., Shi, G., On the gelation of graphene oxide. *J. Phys. Chem. C*, 115, 13, 5545–5551, 2011.
32. Luan, V.H., Tien, H.N., Hoa, L.T., Hien, N.T.M., Oh, E.-S., Chung, J., Kim, E.J., Choi, W.M., Kong, B.-S., Hur, S.H., Synthesis of a highly conductive and large surface area graphene oxide hydrogel and its use in a supercapacitor. *J. Mater. Chem. A*, 1, 2, 208–211, 2013.
33. Wang, D., Kou, R., Choi, D., Yang, Z., Nie, Z., Li, J., Saraf, L.V., Hu, D., Zhang, J., Graff, G.L., Liu, J., Pope, M.A., Aksay, I.A., Ternary self-assembly of ordered metal oxide–graphene nanocomposites for electrochemical energy storage. *ACS Nano*, 4, 3, 1587–1595, 2010.
34. Patil, A.J., Vickery, J.L., Scott, T.B., Mann, S., Aqueous stabilization and self-assembly of graphene sheets into layered bio-nanocomposites using DNA. *Adv. Mater.*, 21, 31, 3159–3164, 2009.
35. Eda, G. and Chhowalla, M., Chemically derived graphene oxide: Towards large-area thin-film electronics and optoelectronics. *Adv. Mater.*, 22, 22, 2392–2415, 2010.
36. Zeng, M., Wang, W.L., Bai, X.D., Preparing three-dimensional graphene architectures: Review of recent developments. *Chinese Phys. B*, 22, 9, 2013.
37. Cao, X., Yin, Z., Zhang, H., Three-dimensional graphene materials: Preparation, structures and application in supercapacitors. *Energy Environ. Sci.*, 7, 1850, 2014.
38. Ji, X., Zhang, X., Zhang, X., Three-dimensional graphene-based nanomaterials as electrocatalysts for oxygen reduction reaction. *J. Nanomater.*, 2015, 1–9, 2015.
39. Compton, O.C., An, Z., Putz, K.W., Hong, B.J., Hauser, B.G., Catherine Brinson, L., Nguyen, S.T., Additive-free hydrogelation of graphene oxide by ultrasonication. *Carbon N. Y.*, 50, 10, 3399–3406, 2012.
40. Bai, H., Li, C., Wang, X., Shi, G., A pH-sensitive graphene oxide composite hydrogel. *Chem. Commun.*, 46, 14, 2376, 2010.
41. Xu, Y., Wu, Q., Sun, Y., Bai, H., Shi, G., Three-dimensional self-assembly of graphene oxide and DNA into multifunctional hydrogels. *ACS Nano*, 4, 12, 7358–7362, 2010.

42. Cong, H.P., Ren, X.C., Wang, P., Yu, S.H., Macroscopic multifunctional graphene-based hydrogels and aerogels by a metal ion induced self-assembly process. *ACS Nano*, 6, 3, 2693–2703, 2012.
43. Chen, W., Li, S., Chen, C., Yan, L., Self-assembly and embedding of nanoparticles by *in situ* reduced graphene for preparation of a 3D graphene/nanoparticle aerogel. *Adv. Mater.*, 23, 47, 5679–5683, 2011.
44. He, G., Tang, H., Wang, H., Bian, Z., Highly selective and active Pd-In/three-dimensional graphene with special structure for electroreduction CO<sub>2</sub> to formate. *Electroanalysis*, 1–11, 2017.
45. Ma, Y. and Chen, Y., Three-dimensional graphene networks: Synthesis, properties and applications. *Natl. Sci. Rev.*, 2, 40–53, 2014.
46. Xie, X., Zhou, Y., Bi, H., Yin, K., Wan, S., Sun, L., Large-range control of the microstructures and properties of three-dimensional porous graphene. *Sci. Rep.*, 3, 1–6, 2013.
47. Sheng, K., Sun, Y., Li, C., Yuan, W., Shi, G., Ultrahigh-rate supercapacitors based on electrochemically reduced graphene oxide for ac line-filtering. *Sci. Rep.*, 2, 1, 247, 2012.
48. Chen, K., Chen, L., Chen, Y., Bai, H., Li, L., Three-dimensional porous graphene-based composite materials: Electrochemical synthesis and application. *J. Mater. Chem.*, 22, 39, 20968, 2012.
49. Zhang, J., Yu, Y., Liu, L., Wu, Y., Graphene-hollow PPy sphere 3D-nanoarchitecture with enhanced electrochemical performance. *Nanoscale*, 5, 7, 3052–7, 2013.
50. Cai, D., Ding, L., Wang, S., Li, Z., Zhu, M., Wang, H., Facile synthesis of ultrathin-shell graphene hollow spheres for high-performance lithium-ion batteries. *Electrochim. Acta*, 139, 96–103, 2014.
51. Shao, Q., Tang, J., Lin, Y., Zhang, F., Yuan, J., Zhang, H., Shinya, N., Qin, L.-C., Synthesis and characterization of graphene hollow spheres for application in supercapacitors. *J. Mater. Chem. A*, 1, 15423–15428, 2013.
52. Wu, L., Feng, H., Liu, M., Zhang, K., Li, J., Graphene-based hollow spheres as efficient electrocatalysts for oxygen reduction. *Nanoscale*, 5, 10839–43, 2013.
53. Huang, X., Qian, K., Yang, J., Zhang, J., Li, L., Yu, C., Zhao, D., Functional nanoporous graphene foams with controlled pore sizes. *Adv. Mater.*, 24, 32, 4419–4423, 2012.
54. Seyyed Monfared Zanjani, J., Saner Okan, B., Letofsky-Papst, I., Yildiz, M., Menciloglu, Y.Z., Rational design and direct fabrication of multi-walled hollow electrospun fibers with controllable structure and surface properties. *Eur. Polym. J.*, 62, 66–76, 2015.
55. Forward, K.M., Flores, A., Rutledge, G.C., Production of core/shell fibers by electrospinning from a free surface. *Chem. Eng. Sci.*, 104, 250–259, 2013.
56. Zanjani, J.S.M., Saner Okan, B., Menciloglu, Y.Z., Yildiz, M., Design and fabrication of multi-walled hollow nanofibers by triaxial electrospinning as reinforcing agents in nanocomposites. *J. Reinf. Plast. Compos.*, 34, 16, 1273–1286, 2015.
57. Shilpa, S., Basavaraja, B.M., Majumder, S.B., Sharma, A., Electrospun hollow glassy carbon-reduced graphene oxide nanofibers with encapsulated ZnO nanoparticles: A free standing anode for Li-ion batteries. *J. Mater. Chem. A*, 3, 10, 5344–5351, 2015.
58. Lin, C.-J., Liu, C.-L., Chen, W.-C., Poly(3-hexylthiophene)/graphene composites based aligned nanofibers for high performance field effect transistors. *J. Mater. Chem. C*, 2015.
59. Promphet, N., Rattanasat, P., Rangkupan, R., Chailapakul, O., Rodthongkum, N., An electrochemical sensor based on graphene/polyaniline/polystyrene nanoporous fibers modified electrode for simultaneous determination of lead and cadmium. *Sensors Actuators B Chem.*, 207, 526–534, 2015.
60. Allen, M.J., Tung, V.C., Kaner, R.B., Honeycomb carbon: A review of graphene. *Chem. Rev.*, 110, 1, 132–145, 2010.

61. Chen, Z., Ren, W., Gao, L., Liu, B., Pei, S., Cheng, H.-M., Three-dimensional flexible and conductive interconnected graphene networks grown by chemical vapour deposition. *Nat. Mater.*, 10, 6, 424–428, 2011.
62. Zhou, M., Lin, T., Huang, F., Zhong, Y., Wang, Z., Tang, Y., Bi, H., Wan, D., Lin, J., Highly conductive porous graphene/ceramic composites for heat transfer and thermal energy storage. *Adv. Funct. Mater.*, 23, 18, 2263–2269, 2013.
63. Ning, G., Fan, Z., Wang, G., Gao, J., Qian, W., Wei, F., Gram-scale synthesis of nanomesh graphene with high surface area and its application in supercapacitor electrodes. *Chem. Commun.*, 47, 21, 5976, 2011.
64. Li, W., Gao, S., Wu, L., Qiu, S., Guo, Y., Geng, X., Chen, M., Liao, S., Zhu, C., Gong, Y., Long, M., Xu, J., Wei, X., Sun, M., Liu, L., High-density three-dimension graphene macroscopic objects for high-capacity removal of heavy metal ions. *Sci. Rep.*, 3, 1, 2125, 2013.
65. Lee, J.-S., Ahn, H.-J., Yoon, J.-C., Jang, J.-H., Three-dimensional nano-foam of few-layer graphene grown by CVD for DSSC. *Phys. Chem. Chem. Phys.*, 14, 22, 7938, 2012.
66. Ito, Y., Tanabe, Y., Qiu, H.J., Sugawara, K., Heguri, S., Tu, N.H., Huynh, K.K., Fujita, T., Takahashi, T., Tanigaki, K., Chen, M., High-quality three-dimensional nanoporous graphene. *Angew. Chemie Int. Ed.*, 53, 19, 4822–4826, 2014.
67. Mao, S., Yu, K., Chang, J., Steeber, D.A., Ocola, L.E., Chen, J., Direct growth of vertically-oriented graphene for field-effect transistor biosensor. *Sci. Rep.*, 3, 33–36, 2013.
68. Wang, H., Shi, L., Yan, T., Zhang, J., Zhong, Q., Zhang, D., Design of graphene-coated hollow mesoporous carbon spheres as high performance electrodes for capacitive deionization. *J. Mater. Chem. A*, 2, 4739–4750, 2014.
69. Luo, J., Ma, Q., Gu, H., Zheng, Y., Liu, X., Three-dimensional graphene-polyaniline hybrid hollow spheres by layer-by-layer assembly for application in supercapacitor. *Electrochim. Acta*, 173, 184–192, 2015.
70. Mao, S., Wen, Z., Kim, H., Lu, G., Hurley, P., Chen, J., A general approach to one-pot fabrication of crumpled graphene-based nanohybrids for energy applications. *ACS Nano*, 6, 8, 7505–7513, 2012.
71. Lee, J.S., Kim, S.I., Yoon, J.C., Jang, J.H., Chemical vapor deposition of mesoporous graphene nanoballs for supercapacitor. *ACS Nano*, 7, 7, 6047–6055, 2013.
72. Huang, X., Qian, K., Yang, J., Zhang, J., Li, L., Yu, C., Zhao, D., Functional nanoporous graphene foams with controlled pore sizes. *Adv. Mater.*, 24, 32, 4419–4423, 2012.
73. Ahn, H.S., Kim, J.M., Park, C., Jang, J.-W., Lee, J.S., Kim, H., Kaviani, M., Kim, M.H., A novel role of three dimensional graphene foam to prevent heater failure during boiling. *Sci. Rep.*, 3, 1, 1960, 2013.
74. Gao, H., Xiao, F., Ching, C.B., Duan, H., High-performance asymmetric supercapacitor based on graphene hydrogel and nanostructured MnO<sub>2</sub>. *ACS Appl. Mater. Interfaces*, 4, 5, 2801–2810, 2012.
75. Chen, P., Yang, J.-J., Li, S.-S., Wang, Z., Xiao, T.-Y., Qian, Y.-H., Yu, S.-H., Hydrothermal synthesis of macroscopic nitrogen-doped graphene hydrogels for ultrafast supercapacitor. *Nano Energy*, 2, 2, 249–256, 2013.
76. Han, Z., Tang, Z., Li, P., Yang, G., Zheng, Q., Yang, J., Ammonia solution strengthened three-dimensional macro-porous graphene aerogel. *Nanoscale*, 5, 12, 5462, 2013.
77. Sun, H., Xu, Z., Gao, C., Multifunctional, ultra-flyweight, synergistically assembled carbon aerogels. *Adv. Mater.*, 25, 18, 2554–2560, 2013.
78. Xu, Z., Li, Z., Holt, C.M.B., Tan, X., Wang, H., Amirkhiz, B.S., Stephenson, T., Mitlin, D., Electrochemical supercapacitor electrodes from sponge-like graphene nanoarchitectures with ultrahigh power density. *J. Phys. Chem. Lett.*, 3, 20, 2928–2933, 2012.
79. Yao, H.-B., Ge, J., Wang, C.-F., Wang, X., Hu, W., Zheng, Z.-J., Ni, Y., Yu, S.-H., A flexible and highly pressure-sensitive graphene-polyurethane sponge based on fractured microstructure design. *Adv. Mater.*, 25, 46, 6692–6698, 2013.

80. Cao, X., Shi, Y., Shi, W., Lu, G., Huang, X., Yan, Q., Zhang, Q., Zhang, H., Preparation of novel 3D graphene networks for supercapacitor applications. *Small*, 7, 22, 3163–3168, 2011.
81. Ferrari, A.C., Meyer, J.C., Scardaci, V., Casiraghi, C., Lazzeri, M., Mauri, F., Piscanec, S., Jiang, D., Novoselov, K.S., Roth, S., Geim, A.K., Raman spectrum of graphene and graphene layers. *Phys. Rev. Lett.*, 97, 18, 2006.
82. Li, W., Gao, S., Wu, L., Qiu, S., Guo, Y., Geng, X., Chen, M., Liao, S., Zhu, C., Gong, Y., Long, M., Xu, J., Wei, X., Sun, M., Liu, L., High-density three-dimension graphene macroscopic objects for high-capacity removal of heavy metal ions. *Sci. Rep.*, 3, 2125, 2013.
83. Sui, Z.Y., Cui, Y., Zhu, J.H., Han, B.H., Preparation of Three-dimensional graphene oxide-polyethylenimine porous materials as dye and gas adsorbents. *ACS Appl. Mater. Interfaces*, 5, 18, 9172–9179, 2013.
84. Bin Yao, H., Ge, J., Wang, C.F., Wang, X., Hu, W., Zheng, Z.J., Ni, Y., Yu, S.H., A flexible and highly pressure-sensitive graphene-polyurethane sponge based on fractured microstructure design. *Adv. Mater.*, 25, 46, 6692–6698, 2013.
85. Shao, Y., El-Kady, M.F., Lin, C.W., Zhu, G., Marsh, K.L., Hwang, J.Y., Zhang, Q., Li, Y., Wang, H., Kaner, R.B., 3D freeze-casting of cellular graphene films for ultrahigh-power-density supercapacitors. *Adv. Mater.*, 6719–6726, 2016.
86. Yang, X., Zhu, J., Qiu, L., Li, D., Bioinspired effective prevention of restacking in multilayered graphene films: Towards the next generation of high-performance supercapacitors. *Adv. Mater.*, 23, 25, 2833–2838, 2011.
87. Wu, Q., Xu, Y., Yao, Z., Liu, A., Shi, G., Supercapacitors based on flexible graphene/polyaniline nanofiber composite films. *ACS Nano*, 4, 4, 1963–1970, 2010.
88. Tan, C., Huang, X., Zhang, H., Synthesis and applications of graphene-based noble metal nanostructures. *Mater. Today*, 16, 1–2, 29–36, 2013.
89. Shi, W., Zhu, J., Sim, D.H., Tay, Y.Y., Lu, Z., Zhang, X., Sharma, Y., Srinivasan, M., Zhang, H., Hng, H.H., Yan, Q., Achieving high specific charge capacitances in Fe<sub>3</sub>O<sub>4</sub>/reduced graphene oxide nanocomposites. *J. Mater. Chem.*, 21, 10, 3422, 2011.
90. Cheng, Q., Tang, J., Shinya, N., Qin, L.C., Co(OH)<sub>2</sub> nanosheet-decorated graphene-CNT composite for supercapacitors of high energy density. *Sci. Technol. Adv. Mater.*, 15, 1, 2014.
91. Li, M., Tang, Z., Leng, M., Xue, J., Flexible solid-state supercapacitor based on graphene-based hybrid films. *Adv. Funct. Mater.*, 24, 47, 7495–7502, 2014.
92. Jahan, M., Bao, Q., Loh, K.P., Electrocatalytically active graphene-porphyrin MOF composite for oxygen reduction reaction. *J. Am. Chem. Soc.*, 134, 15, 6707–6713, 2012.
93. Choi, B.G., Yang, M., Hong, W.H., Choi, J.W., Huh, Y.S., 3D macroporous graphene frameworks for supercapacitors with high energy and power densities. *ACS Nano*, 6, 5, 4020–4028, 2012.
94. Korkut, S., Roy-Mayhew, J.D., Dabbs, D.M., Milius, D.L., Aksay, I.A., High surface area tapes produced with functionalized graphene. *ACS Nano*, 5, 6, 5214–5222, 2011.
95. Niu, Z., Chen, J., Hng, H.H., Ma, J., Chen, X., A leavening strategy to prepare reduced graphene oxide foams. *Adv. Mater.*, 24, 30, 4144–4150, 2012.
96. El-Kady, M.F., Strong, V., Dubin, S., Kaner, R.B., Laser scribing of high-performance and flexible graphene-based electrochemical capacitors. *Science (80)*, 335, 6074, 1326–1330, 2012.
97. Zhang, L., Zhang, F., Yang, X., Long, G., Wu, Y., Zhang, T., Leng, K., Huang, Y., Ma, Y., Yu, A., Chen, Y., Porous 3D graphene-based bulk materials with exceptional high surface area and excellent conductivity for supercapacitors. *Sci. Rep.*, 3, 1, 1408, 2013.
98. Zhang, Y., Chen, P., Gao, X., Wang, B., Liu, H., Wu, H., Liu, H., Dou, S., Nitrogen-doped graphene ribbon assembled core-sheath MnO@graphene scrolls as hierarchically ordered 3D porous electrodes for fast and durable lithium storage. *Adv. Funct. Mater.*, 26, 43, 7754–7765, 2016.

99. Hu, C., Zhao, Y., Cheng, H., Wang, Y., Dong, Z., Jiang, C., Zhai, X., Jiang, L., Qu, L., Graphene microtubings: Controlled fabrication and site-specific functionalization. *Nano Lett.*, 12, 5879–5884, 2012.
100. Wei, X., Li, Y., Xu, W., Zhang, K., Yin, J., Shi, S., Wei, J., Di, F., Guo, J., Wang, C., Chu, C., Sui, N., Chen, B., Zhang, Y., Hao, H., Zhang, X., Zhao, J., Zhou, H., Wang, S., From two-dimensional graphene oxide to three-dimensional honeycomb-like Ni<sub>3</sub>S<sub>2</sub>@graphene oxide composite: Insight into structure and electrocatalytic properties. *R. Soc. Open Sci.*, 4, 12, 171409, 2017.
101. Wang, H., Sun, K., Tao, F., Stacchiola, D.J., Hu, Y.H., 3D honeycomb-like structured graphene and its high efficiency as a counter-electrode catalyst for dye-sensitized solar cells. *Angew. Chemie Int. Ed.*, 52, 35, 9210–9214, 2013.
102. Wang, G., Zhang, L., Zhang, J., A review of electrode materials for electrochemical supercapacitors. *Chem. Soc. Rev.*, 41, 2, 797–828, 2012.
103. Pandolfo, G. and Hollenkamp, F., Carbon properties and their role in supercapacitors. *J. Power Sources*, 157, 1, 11–27, 2006.
104. Ke, Q. and Wang, J., Graphene-based materials for supercapacitor electrode—A review. *J. Mater.*, 2, 1, 37–54, 2016.
105. Qin, K., Liu, E., Li, J., Kang, J., Shi, C., He, C., He, F., Zhao, N., Free-standing 3D nanoporous duct-like and hierarchical nanoporous graphene films for micron-level flexible solid-state asymmetric supercapacitors. *Adv. Energy Mater.*, 1600755, 2016.
106. Fan, W., Xia, Y.Y., Tjiu, W.W., Pallathadka, P.K., He, C., Liu, T., Nitrogen-doped graphene hollow nanospheres as novel electrode materials for supercapacitor applications. *J. Power Sources*, 243, 973–981, 2013.
107. Fan, W., Zhang, C., Tjiu, W.W., Pramoda, K.P., He, C., Liu, T., Graphene-wrapped polyaniline hollow spheres as novel hybrid electrode materials for supercapacitor applications. *ACS Appl. Mater. Interfaces*, 5, 8, 3382–3391, 2013.
108. Yan, Z., Yao, W., Hu, L., Liu, D., Wang, C., Lee, C.-S., Progress in the preparation and application of three-dimensional graphene-based porous nanocomposites. *Nanoscale*, 7, 13, 5563–5577, 2015.
109. Xu, Y., Lin, Z., Huang, X., Liu, Y., Huang, Y., Duan, X., Flexible solid-state supercapacitors based on three-dimensional graphene hydrogel films. *ACS Nano*, 7, 5, 4042–4049, 2013.
110. He, Y., Chen, W., Li, X., Zhang, Z., Fu, J., Zhao, C., Xie, E., Freestanding three-dimensional graphene/MnO<sub>2</sub> composite networks as ultralight and flexible supercapacitor electrodes. *ACS Nano*, 7, 1, 174–182, 2013.
111. Wang, C., Li, Y., Chui, Y.-S., Wu, Q.-H., Chen, X., Zhang, W., Three-dimensional Sn-graphene anode for high-performance lithium-ion batteries. *Nanoscale*, 5, 21, 10599, 2013.
112. Chu, L., Li, M., Wang, Y., Li, X., Wan, Z., Dou, S., Chu, Y., Multishelled NiO hollow spheres decorated by graphene nanosheets as anodes for lithium-ion batteries with improved reversible capacity and cycling stability. *J. Nanomater.*, 2016, 2016.
113. Luo, J., Liu, J., Zeng, Z., Ng, C.F., Ma, L., Zhang, H., Lin, J., Shen, Z., Fan, H.J., Three-dimensional graphene foam supported Fe<sub>3</sub>O<sub>4</sub> lithium battery anodes with long cycle life and high rate capability. *Nano Lett.*, 13, 12, 6136–6143, 2013.
114. Tang, Y., Huang, F., Bi, H., Liu, Z., Wan, D., Highly conductive three-dimensional graphene for enhancing the rate performance of LiFePO<sub>4</sub> cathode. *J. Power Sources*, 203, 130–134, 2012.
115. Bae, S.H., Karthikeyan, K., Lee, Y.S., Oh, I.K., Microwave self-assembly of 3D graphene-carbon nanotube-nickel nanostructure for high capacity anode material in lithium ion battery. *Carbon N. Y.*, 64, 527–536, 2013.
116. Yu, S.X., Yang, L.W., Tian, Y., Yang, P., Jiang, F., Hu, S.W., Wei, X.L., Zhong, J.X., Mesoporous anatase TiO<sub>2</sub> submicrospheres embedded in self-assembled three-dimensional reduced graphene oxide networks for enhanced lithium storage. *J. Mater. Chem. A*, 1, 41, 12750, 2013.

117. Yang, W., Ratinac, K.R., Ringer, S.P., Thordarson, P., Gooding, J.J., Braet, F., Carbon nanomaterials in biosensors: Should you use nanotubes or graphene? *Angew. Chemie Int. Ed.*, 49, 12, 2114–2138, 2010.
118. Yavari, F., Chen, Z., Thomas, A.V., Ren, W., Cheng, H.M., Koratkar, N., High sensitivity gas detection using a macroscopic three-dimensional graphene foam network. *Sci. Rep.*, 1, 1–5, 2011.
119. Kung, C.C., Lin, P.Y., Buse, F.J., Xue, Y., Yu, X., Dai, L., Liu, C.C., Preparation and characterization of three dimensional graphene foam supported platinum-ruthenium bimetallic nanocatalysts for hydrogen peroxide based electrochemical biosensors. *Biosens. Bioelectron.*, 52, 1–7, 2014.
120. Yang, T., Guan, Q., Li, Q.H., Meng, L., Wang, L.L., Liu, C.X., Jiao, K., Large-area, three-dimensional interconnected graphene oxide intercalated with self-doped polyaniline nanofibers as a free-standing electrocatalytic platform for adenine and guanine. *J. Mater. Chem. B*, 1, 23, 2926–2933, 2013.
121. Wang, H., Wang, G., Ling, Y., Qian, F., Song, Y., Lu, X., Chen, S., Tong, Y., Li, Y., High power density microbial fuel cell with flexible 3D graphene–nickel foam as anode. *Nanoscale*, 5, 21, 10283, 2013.
122. Yong, Y.C., Dong, X.C., Chan-Park, M.B., Song, H., Chen, P., Macroporous and monolithic anode based on polyaniline hybridized three-dimensional Graphene for high-performance microbial fuel cells. *ACS Nano*, 6, 3, 2394–2400, 2012.
123. Zhao, S., Li, Y., Yin, H., Liu, Z., Luan, E., Zhao, F., Tang, Z., Liu, S., Three-dimensional graphene/Pt nanoparticle composites as freestanding anode for enhancing performance of microbial fuel cells. *Sci. Adv.*, 1, 10, e1500372–e1500372, 2015.

